c. Surface Properties Engineering

10

Surface Unevenness of Fabrics

Eva Moučková, Petra Jirásková and Petr Ursíny
Technical University of Liberec
The Czech Republic

1. Introduction

Unevenness of plain textile is counted among qualitative parameters of fabric still more often. It shows itself, for example, in the appearance of plain textile (fluttering, cloudy appearance with thick and thin places) as well as in a mass variation of fabric samples. The appearance of plain textiles is influenced by irregularity of yarns that plain textiles are made from and by manufacturing process of plain textile, i.e. by weaving or knitting.
The yarn mass irregularity displays itself in the plain textile by specific known ways (stripiness and a moiré effect). These faults are caused by a periodical irregularity of yarns. A non-periodical yarn irregularity gives cloudiness in the woven or knitted fabric.
Parameters and characteristic functions of mass irregularity (a spectrogram, a variance length curve) are usually used for the evaluation of unevenness of longitudinal textiles (yarns) (Slater, 1986). The parameters indicate a value of irregularity. The characteristic functions describe a structure of mass irregularity and enable to find the causes of irregularity. We can predicate unevenness of plain textile (surface unevenness) on the base of course of the spectrogram as well as the variance length curve. Knowledge of these problems are already known and verified (Zellweger Uster, 1971); (Zellweger Uster, 1988). Currently, there are other possibilities for the prediction of surface unevenness. One of them is the application of so called a *DR* function (Deviation Rate). It is determined, for example, by means of the Uster Tester IV-SX. Today, studies of relation between the magnitude *DR* and surface unevenness are in progress.
Instrumentation used for mass irregularity measurement (for example, the system Oasys from Zweigle, the apparatus Uster-Tester IV-SX from Zellweger Uster) makes, among others, simulation of surface appearance of plain textile (knitted and woven fabric of selected weave) possible. This image is simulated on the basis of signal of measured yarn mass irregularity. This way, the surface appearance of plain textile can be visually evaluated without plain textile manufacturing. But the image evaluation is only subjective in practice because it is realized as a visually judgment of the plain textile appearance.
In the literature (Militký, 2005); (Wegener & Hoth, 1958); (Ursíny et al., 2008); (Suh, 2005), the surface unevenness of plain textile is described by means of the variation coefficient (*CV*) of various properties of plain textile or by means of derived statistical functions. A sample of plain textile is, in these cases, divided into square fields, where individual properties, e.g. mass, are measured. On the basis of results, so-called an area-variation curve is constructed as a parallel to the variance length curve. The area variation curve is constructed also in the works (Suh, 2005); (Moučková & Jirásková, 2006); (Moučková & Jirásková, 2007).

Other statistical functions, by means of them the surface variability is possible to be described, use the fact, that magnitude z(x,y) is a random function of two variables (random field). For example, the co-variation function or so-called directional semivariograms belong to these functions (Militký & Klička, 2005); (Militký et al., 2000); (Militký & Bajzik, 2000).
This chapter summarises obtained experimental knowledge from the problem area of surface unevenness prediction and evaluation. The behaviour of the parameter *DR* in dependence on other parameters and characteristic functions of mass irregularity is studied here. The possibility of utilization of the parameter *DR* for prediction of surface unevenness is analysed. The simulated image of plain textile as well as the image of real woven fabric is used for the surface unevenness evaluation. The simulated appearance of plain textile, obtained from the measuring instrument, is in the greyscale with various intensity of greyness according to yarn irregularity. The image of real woven fabric is obtained by scanning the fabric sample and then is converted into the greyscale. Thus, unevenness of plain textiles (simulated or real) can be converted into unevenness of coloration, which is interpreted by various intensity of grey. A fluctuation of greyness degree in the image is evaluated by means of area variation curves and semivariograms, constructed by means of a special programme created by Militký, J. (Technical University of Liberec) in the programming environment Matlab. Courses of semivariograms are studied in dependence on the woven fabric parameters (the fabric sett, the fabric weave) as well as woven fabric "quality".

2. Structure of yarn mass irregularity and surface unevenness

We find the term "structure of mass irregularity" as components of periodical irregularity expressed by the spectrogram and as non-periodical irregularity in a certain range of yarn length-sections, which expressed external mass irregularity (the variance length function). Newly, the structure of mass irregularity is possible to be described by the *DR* function (Deviation Rate Function) too. The characteristic functions can be used for prediction of some typical forms of surface unevenness (the moiré effect, stripiness, cloudiness).
In following part, we focus on the utilization of *DR* function, eventually its individual values, with the aim of clearing up the relation between this function and other characteristic functions, especially the variance length curve. Thus, we will also be able to illuminate its connection with surface unevenness. The application of *DR* function in mentioned area and also the possibility of surface unevenness quantification is an important assumption for extension of possibilities of surface unevenness prediction based on characteristic functions representing structure of yarn mass irregularity.

2.1 Definition of DR function

The magnitude *DR* and the *DR* function are one of the outputs of the apparatus Uster-Tester IV-SX. The value of *DR* determinates what percentage of the total yarn length exceeds or falls below a pre-set limit of yarn mass deviation (Zellweger Uster, 2001). It is calculated for a certain yarn cut-length. The definition of deviation rate (Zellweger Uster, 2001):

$$DR(x,y)[\%] = \frac{\sum_{i=1}^{k} l_i}{L_{TOT}} \cdot 100 \tag{1}$$

Where: *DR(x,y)* is the deviation rate, sum of parts length l_i [m] of all mass deviation, which are same or higher than ± x [%], relative to total length L_{TOT}[m]; x is the set limit of mass deviation [%]; y is the length of section of fibrous product (yarn), which is used - so-called "cut length" [m]; l_i is the length of "i -th part" of fibrous product (yarn), which surpass the limits ± x [%]; L_T is the total length of fibrous product (yarn), k is number of parts (i = 1, 2, ..., k).

A definite relation between the *DR*-value and the variance-length function (*CV(L)*) results from the definition of *DR* function (Ursíny et al., 2008); (Pinčáková, 2006). It is possible to observe the deviation rate and amount of mass variability in various length sections (cut lengths).

2.2 Definition of area variation curve

The area variation curve describes the variability of greyness degrees (i.e. unevenness of plain textile image) in dependence on square field area. It can be expressed as an external or an internal curve. The curve is a certain analogy of the variance-length curve, because it has similar character of behaviour. The internal area variation curve is expressed by the variation coefficient of greyness degree inside square area in dependence on the area of observed square field. This curve increases with growing area of square field. The external variation curve shows the variability of greyness degree between square field areas of image. The curve slopes down with growing area of square field (see Fig. 1.).

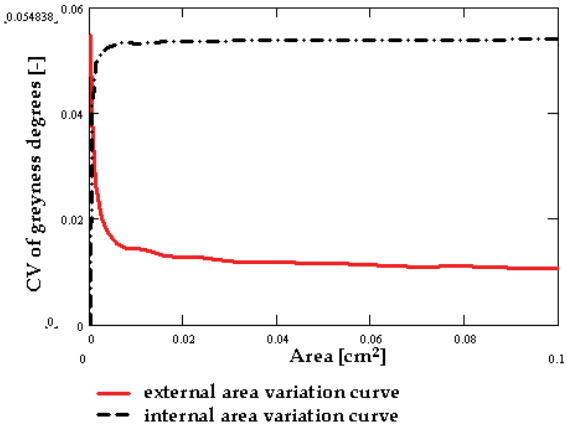

Fig. 1. Area variation curves – example

In this work, the external area variation curve is calculated by the formula:

$$CV(A) = \frac{S(A)}{\overline{\overline{X}}(A)} \tag{2}$$

Where: *CV(A)* is the external variation coefficient of average greyness degrees between square fields of the area A in the fabric image; *S(A)* is the standard deviation of mean values of greyness degrees in square fields of the area A included in a fabric image; $\overline{\overline{X}}(A)$ is the mean value from all mean values of greyness degrees in square fields of the area A.

2.3 Experimental results

Within the experiment, a combed yarn (100 % CO, count of T = 16.5 tex) and a carded yarn (100 % CO, count of T = 25 tex) have been used for the evaluation of unevenness in plane (surface unevenness). The possibility of utilization of parameter *DR* for prediction of surface unevenness is analysed too. The yarns have been measured on the apparatus Uster Tester IV-SX, where parameters $CV_m(1m)$ [%] and $DR(5\%;1.5m)$ [%], the spectrogram and the variance-length curve have been observed. It has been done 20 measurements for each type of yarn (Ursíny et al., 2008), (Pinčáková, 2006).

The dependence of the $DR\ (5\%;\ 1.5\ m)$ [%] values on values of $CV_m(1\ m)$ [%] has been studied. Selected results are mentioned in the Fig. 2. The linear dependence is evident between observed magnitudes. The correlation coefficient r is equal to 0.9725 in the case of tested combed yarns. In the case of carded yarns the correlation coefficient is 0.6929.

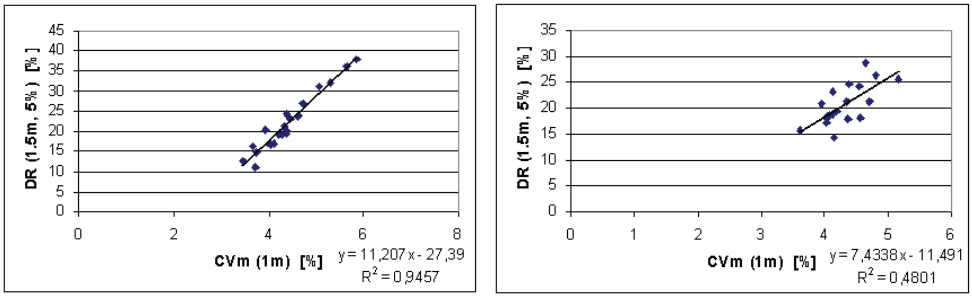

(a) Combed yarn (b) Carded yarn

Fig. 2. Relation between $DR\ (5\%;\ 1.5\ m)$ [%] and $CV_m\ (1m)$ [%] values

The relation between *DR*-value and the spectrograms and the variance-length function of combed yarns has been observed too. The results have been confronted with simulated appearances of woven fabrics generated by the Uster-Tester IV-SX. The courses of characteristic functions for selected combed yarns (see the Table 1) are mentioned in the Fig. 3. The examples of simulated fabric appearances are shown in the Fig. 4.

Measurement No.	CV_m (1m) [%]	DR (5%; 1,5 m) [%]
2071	5.85	38
2070	4.33	21.2
2069	4.37	19.4
2068	4.23	19
2067	4.38	20.2

Table 1. Selected parameters of mass irregularity – selected measurements - combed yarn

From the courses of the variance-length curves for the selected set of 5 tested combed yarns (Fig. 3a), it is evident, that the yarn measurement No. 2071 shows an accrual of irregularity (the cut length of 1 m – 10 m). The yarn shows worse irregularity also in the spectrogram (Fig. 3b), where the periodical irregularity is recorded on the wave- lengths of 3 m and 7 m.

The simulated images created from combed yarns, which have higher mass irregularity (*CV*), worse spectrogram as well as the variance length curve, shows worse appearance. It is

more unsettled (level of greyness degree fluctuates). In the case of weaves denim and satin there were visible differences in the appearance of individual images.

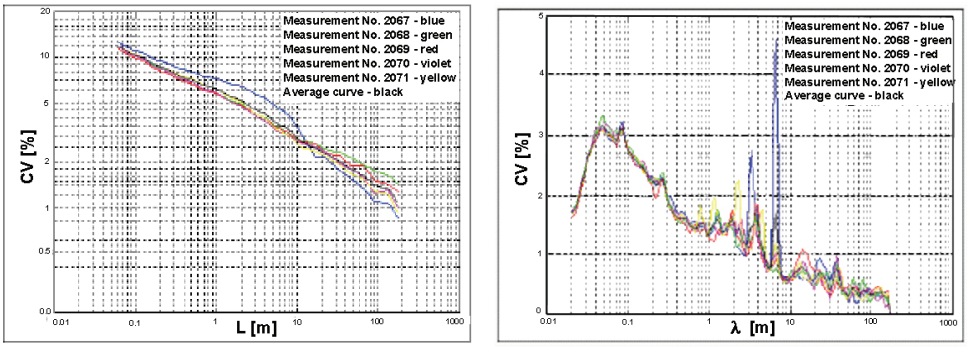

(a) Variance- length curves (b) Spectrograms

Fig. 3. Variance-length curves and spectrograms of combed yarn (100%CO, yarn count of 16.5 tex)

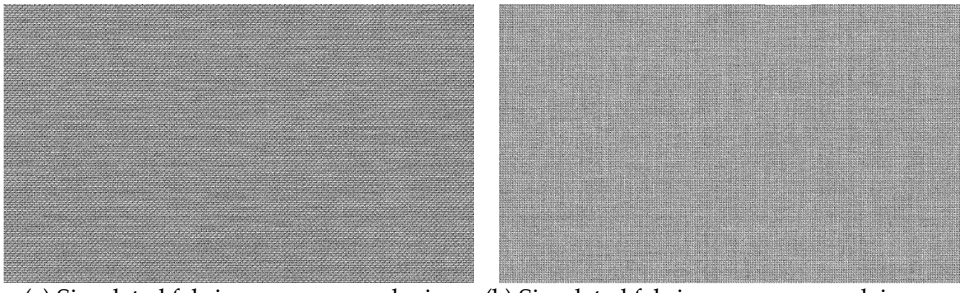

(a) Simulated fabric appearance – denim weave (b) Simulated fabric appearance – plain weave

Fig. 4. Simulated appearances of woven fabrics. Combed yarn. Measurement No. 2071. Real size of image – 15.54 x 9.29 cm. Resolution 300 dpi.

The visual assessment of yarn taper board simulation, generated by the apparatus Uster Tester IV-SX (for example see the Fig. 5.), has been used as an auxiliary evaluation.

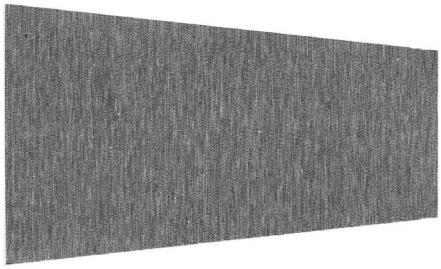

Fig. 5. Simulated yarn board from the Uster-Tester IV – SX. Combed yarn. Measurement No. 2071

In the case of the yarn No. 2071 (see the Table 1), a moiré effect tendency has been registered there (Fig. 5). The appearance of this yarn seems to be the worst. The moiré effect has not been observed on the other yarn boards, total yarn appearance seems to be better (less unsettled). Higher number of neps was evident from appearances of all yarns.
Obtained images of fabrics appearances have been evaluated not only visually (the subjective method) but by means of the area variation curve too. The curve is one of results of the mentioned special script made by Militký. The program constructs this curve according to the formula (2). An influence of yarn mass irregularity on the appearance of simulated woven fabric image has been observed. Selected area variation curves of greyness degrees of simulated woven fabric appearance are mentioned in the Fig. 6 and Fig. 7.

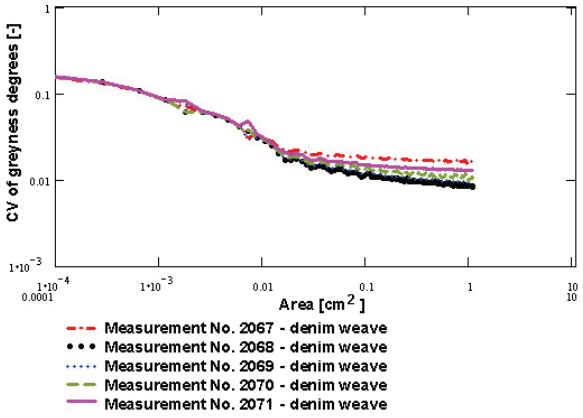

Fig. 6. Area variation curves of greyness degrees of fabric appearances simulated from irregularity measurements - combed yarn. Curves of fabrics with denim weave

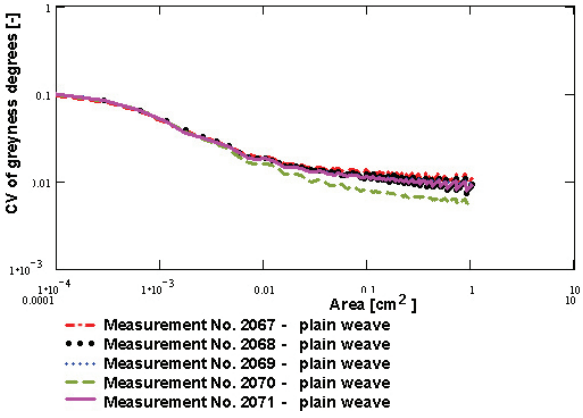

Fig. 7. Area variation curves of greyness degrees of fabric appearances simulated from irregularity measurements - combed yarn. Curves of fabrics with plain weave.

Differences between courses of area variation curves were insignificant in the case of the plain weave. High density of this weave is probably a reason of difficult surface unevenness

identification, because the plain weave does not have so called a float thread and so mass irregularity of yarn hides up. In the case of weave, that are not so dense (the denim weave, the satin weave), differences in the appearance of flat textile are visible and identifiable. The appearance of flat textile corresponds with measured values of yarn irregularity and yarn appearance more. The yarn, that showed higher *CV* value, worse spectrogram as well as the course of the variance-length curve, had worse appearance of simulated fabric too – see the measurement No. 2071 where the curve is deflected up. In the case of these weaves, yarn irregularity does not hide and it is identifiable on the float thread. If courses of both variance-length curve and spectrogram are faultless, behaviours of area variation curves are nearly congruent.

Total observed area of simulated fabrics image has been divided into square fields during construction of the area-variation curves. The area of square field gradually increased (from several pixels to several thousands of pixels). The area of evaluated square has an influence on the value of variability of greyness degree. This value decreases with increasing area of square field, but simultaneously number of square fields, i.e. number of measurements, grades down. Stability of ascertained results corresponds with this fact. It shows itself by "a saw-toothed" course of area variation curve. For results reliability, a certain minimal number of square fields is necessary; therefore the evaluated area of one square was at the most of 1cm^2.

3. Utilization of semivariograms for surface unevenness evaluation

3.1 Definition of semivariograms

The semivariogram expresses spatial dissimilarity between values at point x_i and x_j. Generally, it is defined as one-half variance of differences ($z(x_i)$ - $z(x_i+lag)$) (Cressie, 1993); (Militký et al, 2000); (Březina & Militký, 2002); (Militký & Klička, 2005):

$$\Gamma(lag) = 0,5 \,.D(z(x_i) - z(x_i + lag)) \tag{3}$$

The magnitude ***lag*** is a directional vector (0°; 90°, 45°) representing separation between two spatial locations. For uniformly distributed points, x values of vector ***lag*** express the multiples of distance between squares in direction of columns (0°), rows (90°) and diagonals (45°) (Militký & Klička, 2005). Thus, 3 types of semivariograms are obtained (in direction of columns, rows and diagonals). Omni-directional semivariogram is calculated by averaging of all 3 types of semivariograms. For stationary random field the mean value is constant in individual locations. Then this formula holds (Cressie, 1993); (Militký et al, 2000):

$$\Gamma(lag) = 0,5 \,.E(z(x_i) - z(x_i + lag))^2 \tag{4}$$

If $\Gamma(lag)$ = const., the magnitude $z(.)$ is not correlated in the given direction. When a random field is non-stationary (average value in each field is not constant) it is possible to construct so called a centred sample semivariogram (Militký et al., 2000), which has been used in this work:

$$G(lag) = \frac{1}{2N(lag)} \sum_{i=1}^{N(lag)} (z_c(x_i) - z_c(x_i + lag))^2 \tag{5}$$

Where: $z_c(x_i)$ is the centred average greyness degree defined as:

$$z_c(x_i) = z(x_i) - \frac{\sum_{i=1}^{n(x_i)} z(x_i)}{n(x_i)} \tag{6}$$

N*(lag)* is number of pairs of observations separated by distance *lag; z(x_i)* is greyness degree in the location x_i. The woven fabric image is divided into square fields like a net. The centres of fields are the locations x. The average value of greyness degree in the given square field is assigned to the location x ($z(x_i)$).

3.1.1 Exemplary courses of semivariograms

For the prefaced of semivariograms problems, semivariograms from greyness degrees of exemplary images, made by authors, have been constructed. These images are mentioned in the Fig. 8. Size of each image is 200 x 200 pixels. The resolution is 200 dpi. The fabric images without frame have been processed by means of the mentioned special script made by Militký. The programme converts the fabric image to the greyness degrees and, in the case of the semivariogram, divides it in to square fields of selected size *step x step* pixels. The average greyness degree *($z(x_i)$)* is calculated in each field. From obtained values the centred semivariogram in given direction is calculated according to the formula (5), see Fig. 8.
From semivariograms, it is possible to identify stripiness of the image pursuant to courses of the semivariogram in rows direction together with the semivariogram in direction of columns. So, it was decided to use semivariograms for analysis of surface unevenness of woven fabric.

3.2 Experiment and results

For experiment there were used:

- Woven fabric images simulated by means of the Uster-Tester IV-SX apparatus on the basis of measurement results of yarn mass irregularity. Yarns with various level of irregularity have been used.
- Real fabric samples with various weft sett, weave and quality.

The images of real fabrics have been obtained by scanning of fabric samples. The samples have been covered with the black as well as the white underlay during scanning for better identification of surface unevenness. All obtained fabric images have been processed by means of the mentioned special script. An influence of the fabric sett, the fabric weave as well as fabric quality on the behaviour of semivariograms has been observed.

3.2.1 Semivariograms of fabric images simulated on the Uster-Tester apparatus

The instrumentation Uster Tester IV-SX enables to simulate woven and knitted fabric appearances as well as a yarn board on the base of yarn mass irregularity measurement. Obtained appearances are in the grey scale, which has various intensity of greyness degree according to structure of yarn mass irregularity.
For experiment 100%CO rotor yarns have been used. Count of these yarns was 55 tex, machine twist was 625 tpm. Three yarns had been manufactured. Two of them had been produced purposely with faults. For the first case, a bad sliver had been used (the measurement No. 3398) and for the second case, an impurity has been inserted into the rotor groove of machine to produce yarn with moiré effect (the measurement No. 4192). Yarn mass irregularity has been measured on the apparatus Uster Tester IV-SX. Selected parameters of yarn mass irregularity are mentioned in the Table 2.

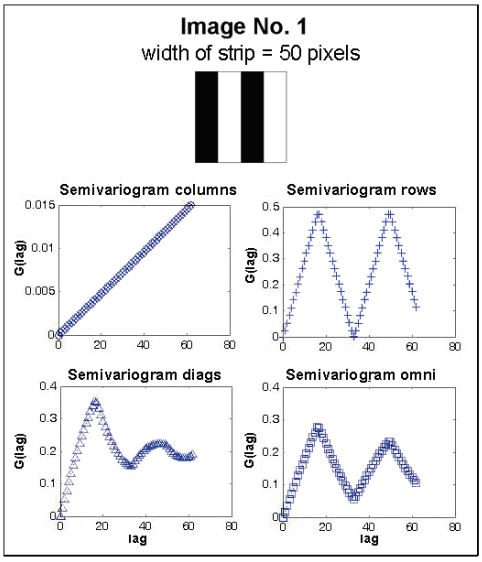

(a) Exemplary image and corresponding semivariograms

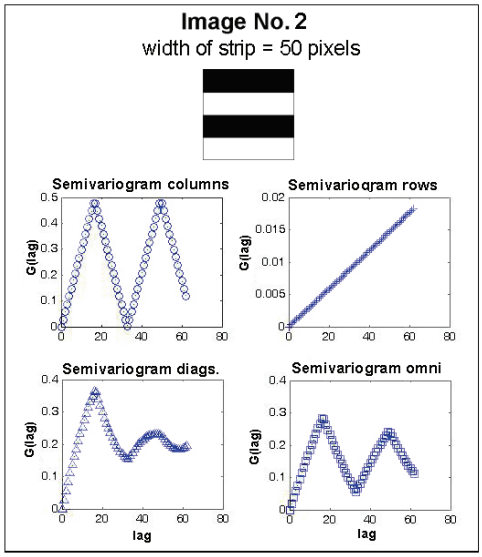

(b) Exemplary image and corresponding semivariograms

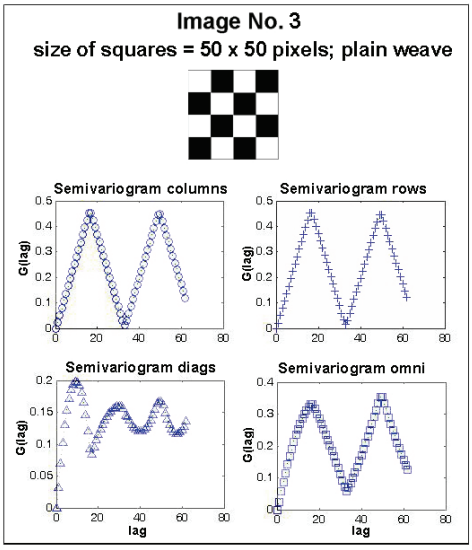

(c) Exemplary image and corresponding semivariograms

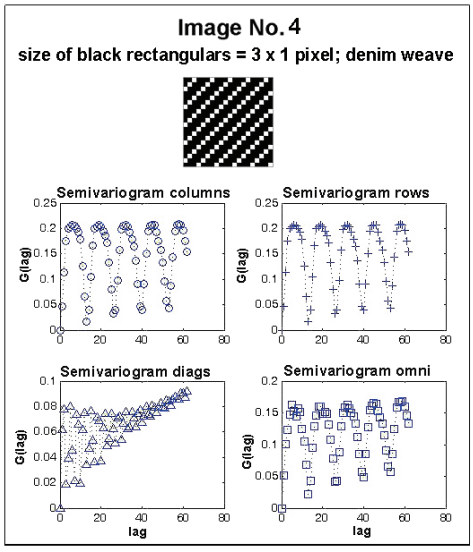

(d) Exemplary image and corresponding semivariograms

Fig. 8. Semivariograms from greyness degrees of images – used whole images without frame, set step = 3 pixels

Measurement No.	U [%]	CV [%]	CV(1m) [%]	CV(3m) [%]	CV(10m) [%]	Thin places –50% [1/km]	Thick places +50% [1/km]	Neps +280% [1/km]
3396	10,86	13,71	4,29	3,93	3,70	2,5	57,5	42,5
3398	11,13	14,17	7,98	6,79	5,18	2,5	77,5	57,5
4192	25,30	38,02	3,43	2,75	2,48	2373	6368	5738

Table 2. Selected parameters of yarn mass irregularity

For spectrograms of these yarns see the Fig. 9a-c, for variance length curves see the Fig. 10a-c.

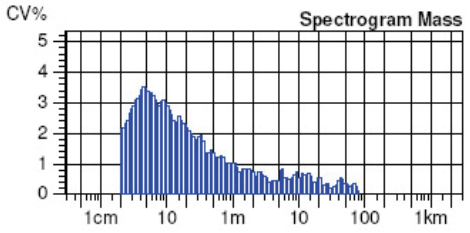

(a) Measurement No. 3396

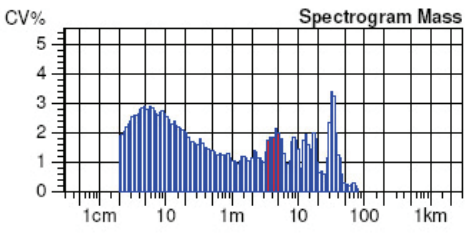

(b) Measurement No. 3398

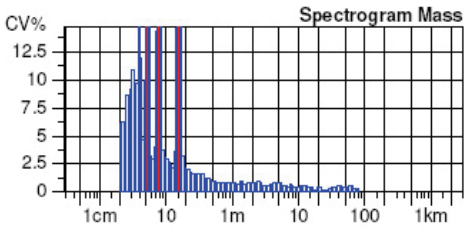

(c) Measurement No. 4192

Fig. 9. Spectrograms of yarns

It is evident (Fig. 9a), the yarn No. 3396 has short-term irregularity on wavelengths λ = (4 - 6) cm, the shape of spectrogram embodies no other faults. The spectrogram of yarn No. 3398 (Fig. 9b) has increased amplitude on wavelength λ = 35 m and draft waves on wavelengths λ = (4; 9; 15) m. Because of drafting waves in the spectrogram, yarn wound on the board as well as the image of flat textile should show disturbed appearance, so called cloudiness. The stripiness should be shown in the flat textile due to higher periodic irregularity on the wavelength λ = 35 m.

From the spectrogram of yarn No. 4192 (Fig. 9c) it is evident the moiré effect – higher amplitudes on wavelengths λ = (16; 8; 5) cm. Increased amplitude on the basic wavelength (16 cm) corresponds to the rotor circumference (rotor diameter d = 53 mm), wavelengths of other higher amplitudes correspond to wavelengths $\lambda/2$ and $\lambda/3$. It means the yarn wound on the black board will have the moiré effect caused by impurities in the rotor groove.

The variance-length curve of yarn No. 3396 (Fig. 10a) shows gradual decrease of CV values with increasing cut length. This decrease is rapider on the cut lengths L = (2 – 20) cm. The

curve of yarn No. 3398 (Fig. 10b) falls more slowly up to the cut length L = 10 m, then rapid decrease of the curve follows. Increased values of CV on higher cut lengths (L = 1 – 10 m) indicate cloudiness of future flat textile. The variance-length curve of yarn No. 4192 (Fig. 10c) has markedly higher values of CV on cut lengths L = 2 cm – 1 m, its decrease is the rapidest up to the length of 1m compare to the previous curves. Higher values of CV up to the cut length L = 1 m predicate short disturbing faults in the flat textile.

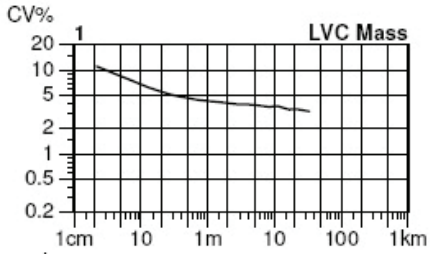

(a) Measurement No. 3396

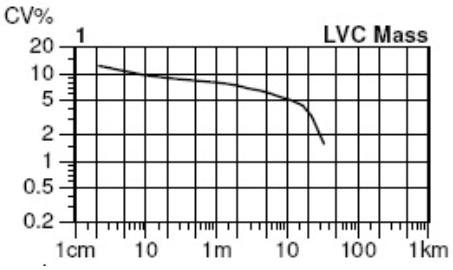

(b) Measurement No. 3398

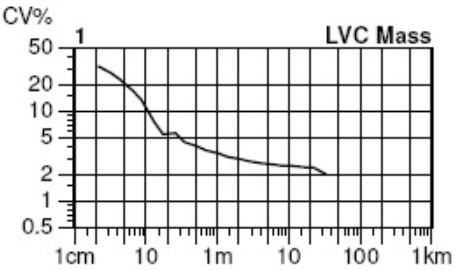

(c) Measurement No. 4192

Fig. 10. Variance-length curves of yarns

The appearance of the flat textile – the woven fabric (plain, satin and denim weave) and the yarn board has been simulated on the basis of measured data of yarn mass irregularity by the apparatus Uster-Tester IV-SX. There are yarn boards and appearances of woven fabrics in the denim weave for selected measurement in the Fig. 11 – Fig. 13.

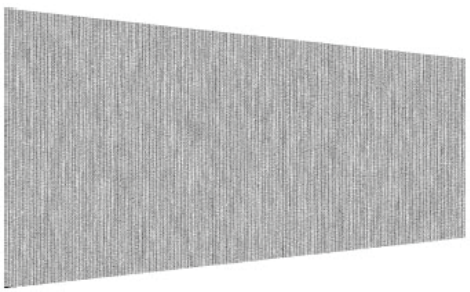

(a) Yarn board

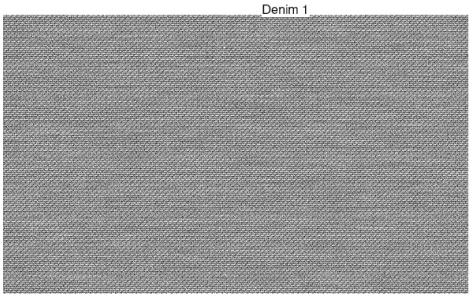

(b) Woven fabric appearance

Fig. 11. Simulated images of yarn board and woven fabric appearance with denim weave – (Real size of image – 15.54 x 9.29 cm. Resolution 300dpi) - Measurement No. 3396

Visually, the appearance of woven fabric with denim weave from the measurement No. 3396 seems to be similar to the appearance of woven fabric from the measurement No. 3398 at first sight. But seen in close-up, the woven fabric from the yarn No. 3398 has slightly worse appearance. This yarn shows slightly higher *CV* values, worse shape of the spectrogram and the variance-length curve in comparison to the yarn No. 3396. Woven fabric from the yarn No. 4192 has the worst appearance clearly caused by higher yarn mass irregularity (*CV*) and by the worst spectrogram as well as the variance length curve. The moiré effect is obvious on the yarn board (see Fig. 13a), but it is disturbed by weave in the fabric. The fabric appearance is unsettled (Fig. 13b).

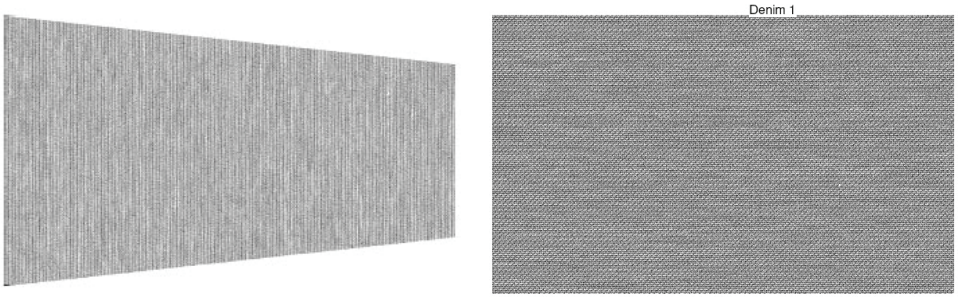

(a) Yarn board (b) Woven fabric appearance

Fig. 12. Simulated images of yarn board and woven fabric appearance with denim weave – (Real size of image – 15.54 x 9.29 cm. Resolution 300 dpi) - Measurement No. 3398

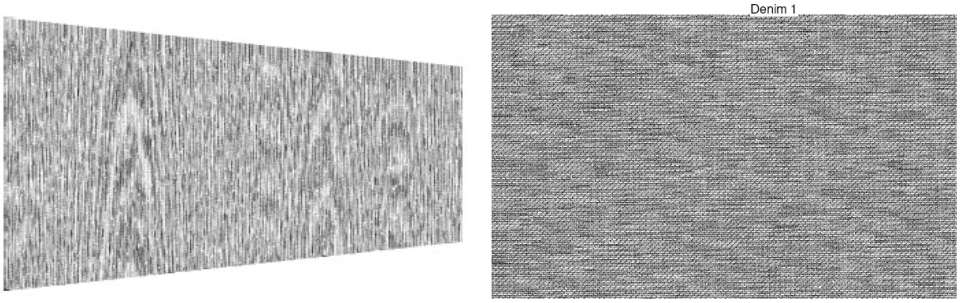

(a) Yarn board (b) Woven fabric appearance

Fig. 13. Simulated images of yarn board and woven fabric appearance with denim weave - (Real size of image – 15.54 x 9.29 cm; resolution 300 dpi) – Measurement No. 4192

These images have not been evaluated only visually, but also by means of the above-mentioned script. The size of observed image was 1000 x 1000 pixels (resolution 300 dpi, i.e. c. 8.5 x 8.5 cm).

Two types of semivariograms in the given direction have been constructed. In the first case, section of each image with size of 1000 x 1000 pixels has been observed. The step of 60 pixels has been chosen. It corresponds to real size of c. 0.5 cm. See the Fig. 14, where semivariograms of fabric image with the denim weave are mentioned. From the semivariograms it is evident, that the curve of image from the yarn No. 3396 has the best

course. This yarn has got the best values in term of parameters of yarn mass irregularity. The semivariograms of this image are nearly constant from *lag* = 3 in all directions. It means, observed square fields of the image are similar to each other in term of average centred greyness degree. So, neither cloudiness nor stripiness was not record. It corresponds to visual evaluation of the image. The semivariograms of image from the yarn No. 3398 shows higher values compared to the curve of yarn No. 3396. Its course is similar to the course of the curve of yarn No. 3396 in direction of columns. They are nearly identical in direction of rows. By visual evaluation of woven fabric appearances, any marked differences between images from yarns No. 3396 and No. 3398 have not been found. But semivariograms were probably able to record colour differences in the images caused by slowly increased mass irregularity and drafting waves of the yarn. The curves of all types of semivariograms of the yarn No. 4192 very fluctuate, also show markedly higher values compare to curves of the image from other two yarns. It is possible to say, the character of curve corresponds to visual evaluation of the image – strongly unsettled appearance of the woven fabric.

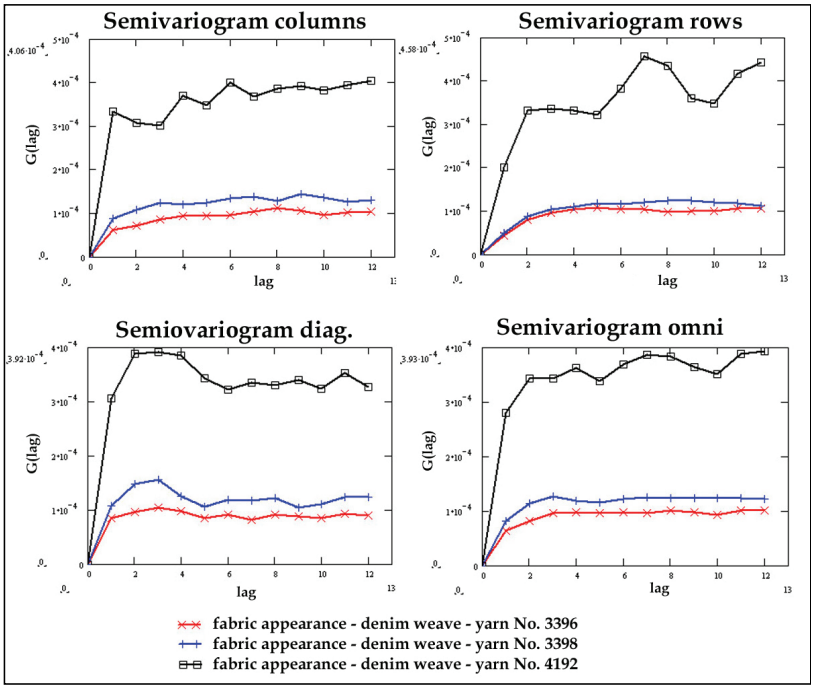

Fig. 14. Semivariograms from greyness degrees – simulated image of woven fabric – denim weave 3/1 – observed size: 1000 x 1000 pixels; step: 60 pixels

In the second case, sections of each image with size of 118 x 118 pixels from the centre of image have been observed. The step of 2 pixels has been chosen. An influence of fabric weave on the course of semivariogram has been observed (see the Fig. 15).
Semivariograms mentioned in the Fig. 15 does not record whole image, but they analyse only area of 118 x 118 pixels, i.e. 1 x 1 cm of the image. By observing of small section of the fabric image, it is possible to identify the fabric weave from courses of semivariogram in direction of rows and columns – in this case the denim (twill 3/1). It has been verified. You

can compare semivariograms in the direction of row and columns in the Fig. 15 and the course of semivariograms in the Fig. 8, where exemplary semivariograms for the denim weave are shown. The denim is a weave characteristic by line spacing. Maximums and minimums in the semivariograms (Fig. 15) correspond to the spacing. The position of semivariogram curve is influenced by yarn irregularity. The yarn No. 4192 has the highest *CV* on short wavelengths. It expresses itself as quickly changing of dark and white sections in the image. That way the semivariogram curves of these images have the highest values. Courses of semivariograms of all yarns in all directions are similar.

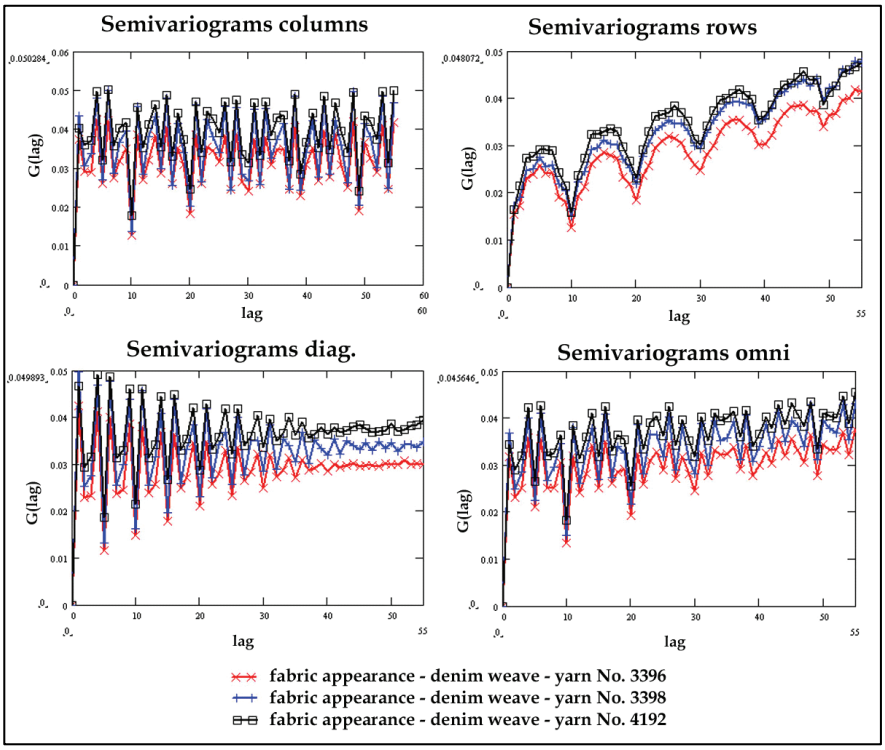

Fig. 15. Semivariograms from greyness degrees – simulated image of woven fabric – denim weave 3/1 – observed size: 118 x 118 pixels; step: 2 pixels

3.2.2 Semivariograms of real tested fabric samples

In this part, the courses of semivariograms of greyness degrees of real fabric samples with various weft sett, weave and quality are presented. For the first experiment with real fabric samples, white colour woven fabrics (100 % CO) of the plain weave have been used. Warp and weft yarn count was 33 tex. The fabrics with three level of weft density have been used. The density was: 16 threads/1cm (the fabric marked B16), 20 threads/1cm (the fabric marked B20) and 24 threads/1cm (the fabric marked B24). The yarn used for these fabrics show neither bad course of spectrogram or variance-length curve. Therefore we can expect settled fabric appearance with low greyness degree fluctuation. The images of woven fabric

necessary for semivariogram construction have been obtained by scanning of 12 samples from each fabric. The image resolution was 200 dpi. The samples have been scanned with a black as well as a white underlay. By putting of a black paper onto the scanned sample the black underlay has been created, whereas for the white underlay the sample has been covered by sheet of white paper. The real size of observed image was 15 x 21 cm (i.e. 1181 x 1653 pixels), for illustration see the Fig. 16.

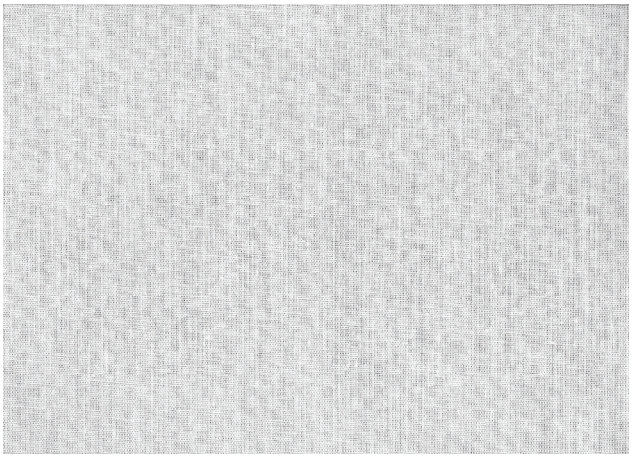

Fig. 16. Image of the real woven fabric B16; sample 1.1; the black underlay. Size of whole image: 1181 x 1653 pixels, resolution: 200 dpi

The real fabric images have been processed by mentioned special script to the „centred" semivariograms of greyness degree be obtained. The area of 1170 x 1170 pixels has been observed in the sample. The step of 20 pixels (corresponding to 0.25 cm) had been selected. The average semivariograms have been constructed in given direction (columns, rows, diagonals, omni) for each type of woven fabric. They are shown in the Fig. 17 and Fig. 18. An influence of the fabric sett on the course of the semivariogram has been observed in this experiment. These semivariograms show, that the methodology of scanning influences their courses. The white underlay of scanning fabrics does not seem to be suitable due to low contrast of image. The fabric trans-illumination does not evince itself on the background. The black underlay is better, thus the image with this underlay have been evaluated. From the semivariograms in the Fig. 18 it is evident the average greyness degrees in the squares of area 20 x 20 pixels (size of the step) are not correlated from c. $lag = 10$ in any direction. In the case of smaller distance of squares ($lag < 10$), semivariograms are convex ascending. These semivariograms do not show any stripiness. By visual evaluation of fabric samples any stripiness has not been evident too.

It was found out the fabric sett influences the level of semivariograms values. The values corresponding to the fabric of higher weft sett (the fabric B24) were lower in comparison with semivariograms of fabric with lower weft sett (the fabric B16). It is due to the black underlay, which was put on the fabric before scanning. In the case of the fabric of lower weft sett, this underlay strikes more through the fabric during scanning than in the case of the fabric of higher weft sett. This problem is described in the authors` work (Moučková & Jirásková, 2008).

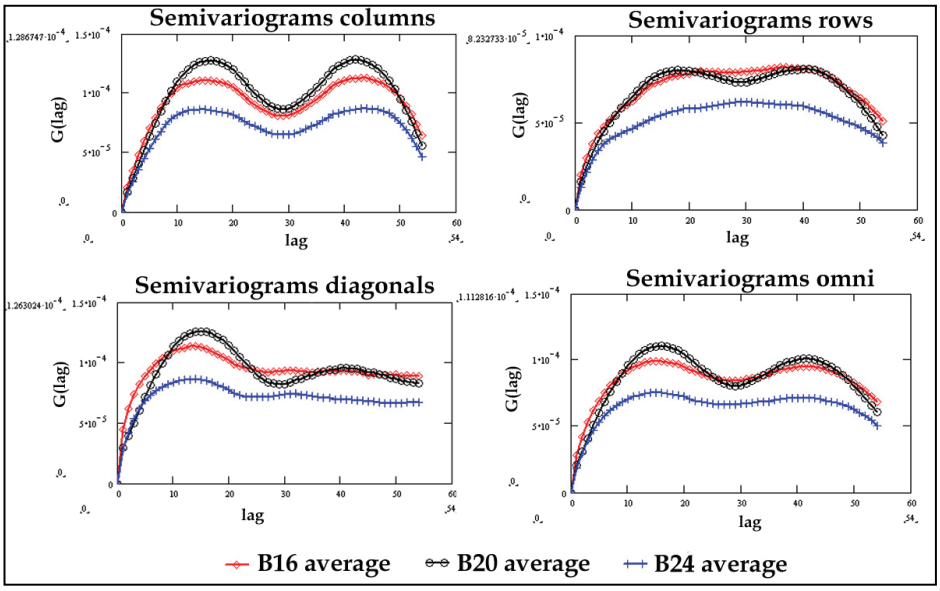

Fig. 17. Average semivariograms – real fabric images - plain weave – observed area: 1170 x 1170 pixels, step: 20 pixels, the white underlay

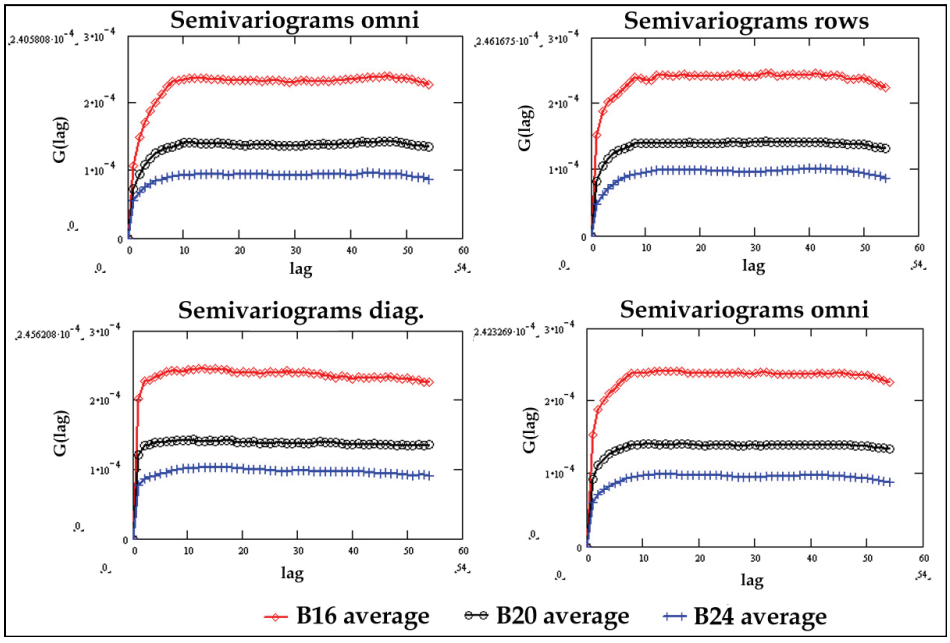

Fig. 18. Average semivariograms – real fabric images - the plain weave – observed area: 1170 x 1170 pixels, step: 20 pixels, the black underlay

Woven fabrics of various weaves have been used for the second experiment. Selected parameters of these fabrics are mentioned in the Table 3.

Fabric weave	Weft sett (threads/10cm)	Warp sett (threads/10cm)	Yarn fineness in the warp and weft [tex]	Raw material
Satin 1/7 (5)	350	388	14,5	100%CO
Twill ½ (Z)				
Twill 5/5 (Z)				
Plain				
Hopsack 2/2				

Table 3. Selected parameters of used woven fabrics

The fabrics had been manufactured both in a standard way and with a fault (stripiness in the direction of warp) on the same loom. The stripes had been obtained during warping. The yarn bobbins, produced in different spinning lot, had been set on the half of the creel. The parameters of these yarns had been the same, but the colour shade of cotton has differed. Six samples have been taken from each fabric for experiment

The fabric samples of size 15 x 21 cm have been scanned with resolution 300 dpi from the face of fabric with black underlay to obtain fabric image – for example see the Fig. 19 and the Fig. 20.

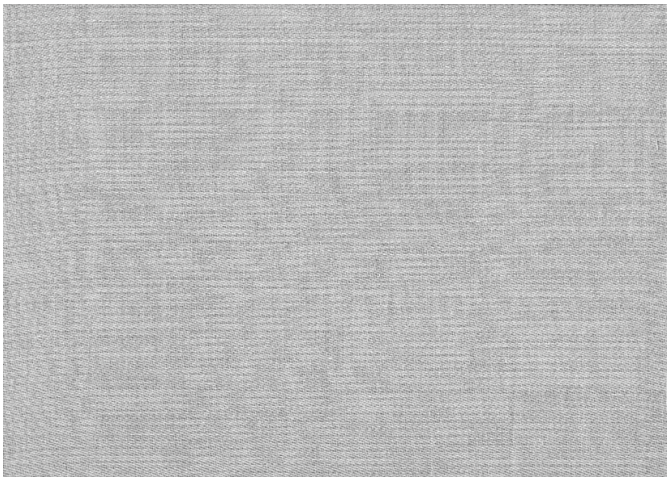

Fig. 19. Image of normal fabric - the weave satin 1/7. Real size of image: 15 x 21 cm; resolution: 300 dpi

The semivariograms in the given direction have been constructed. The section of each image with size of 1700 x 1700 pixels has been observed. The step of 60 pixels has been chosen. The courses of semivariograms according to fabric quality have been observed - see Fig. 21. From this figure it is evident that semivariograms in the direction of rows record stripes in the fabrics. The fabric samples with stripes had c. 6.5 stripes in direction of warp in evaluated area. The width of two stripes next to each other was 46 mm. It corresponds to

544 pixels in the fabric image. At the step of 60, the distance between outside squares of repetitious stripes of the same colour shade was equal to 9 (544/6) - which corresponds to period Δlag = 9 in the curve.

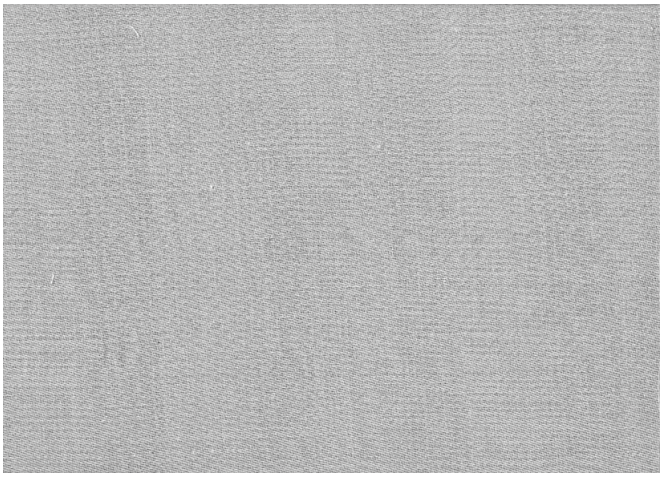

Fig. 20. Image of fabric with stripes – the weave satin 1/7. Real size of image: 15 x 21 cm; resolution: 300 dpi

A specimen example has been constructed for verification of this assertion. The square of size 1700 x 1700 pixels with resolution of 300 dpi containing vertical stripes of width 23 mm (272 pixels) has been drown. This image has been treated by mentioned programme at the same setting as in the case of fabric. See results on the Fig. 22.
The semivariogram in the direction of rows has a periodical course. At the step of 60 pixels, the period is 9. This period corresponds to 544 pixels in the image (i.e. 46 mm) and so to distance between edges of stripes of the same colour shade. The semivariogram in the direction of columns has linearly growing course.
It was verified that combination of semivariograms in the direction of rows and in the direction of columns seems to be suitable tool for recording of periodical unevenness – stripiness of woven fabric.

4. Conclusion

The structure of mass irregularity described by characteristic functions (the spectrogram, the variance-length curve, the *DR* function) influences surface unevenness by specific way. Periodical irregularity, presented by the spectrogram, causes surface unevenness, which is distinguished by a certain geometrical regularity (moiré effect, stripiness). Non-periodical irregularity expressed by the variance-length curve and by the *DR* function leads to a surface unevenness, which, on the contrary, can be characterized by geometrical non-uniformity (cloudiness). The experimental measurements have showed that the linear dependence exists between measured values of *DR (5%, 1.5m)* and $CV_m(1m)$. Ascertained high value of correlation coefficient confirms it. This value highly exceeds a critical value

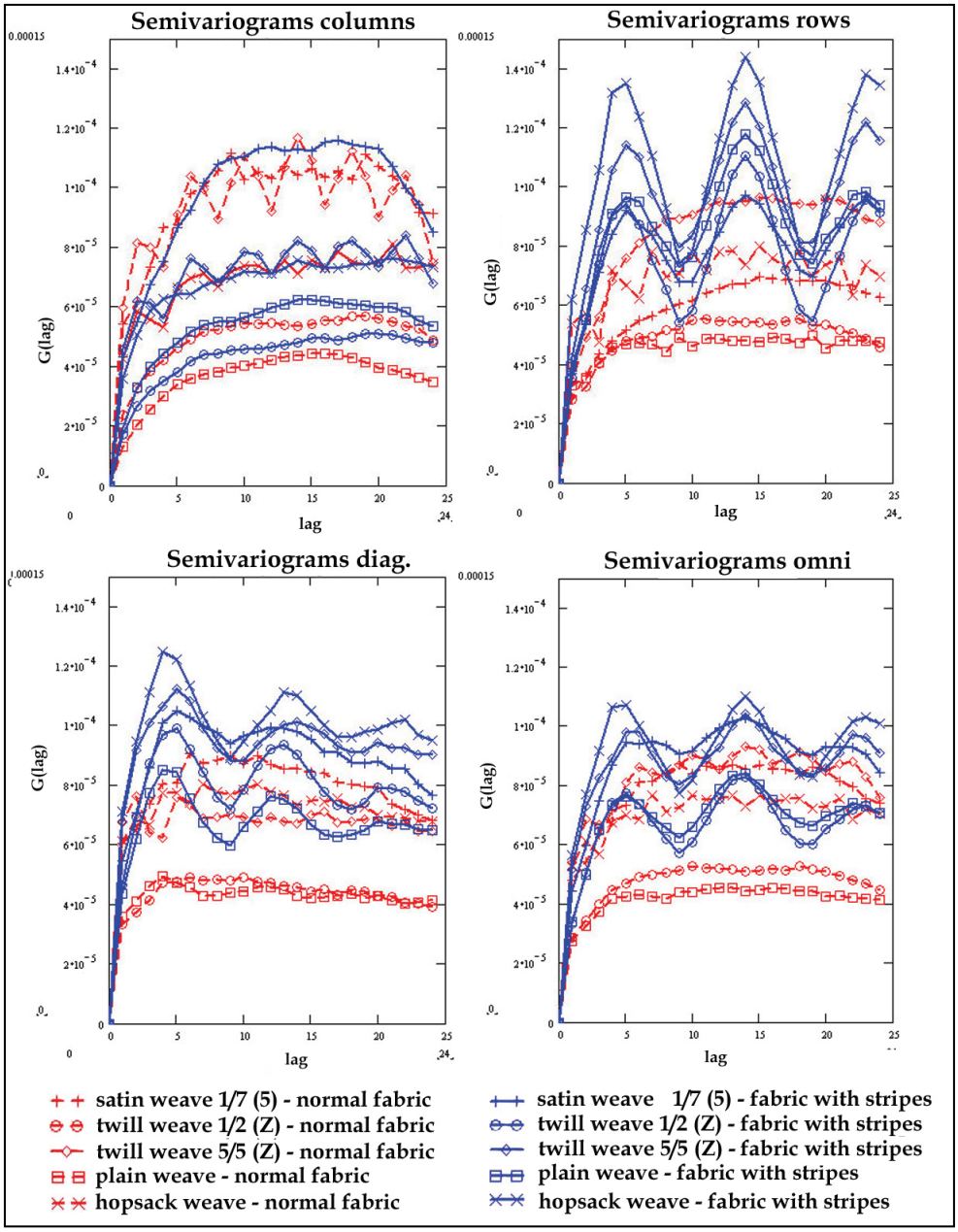

Fig. 21. Semivariograms of normal and stripped fabrics – observed sample area: 1700 x 1700 pixels; step: 60 pixels

also in the case of the confidence limit of 99%. Hitherto knowledge about relation between the variance-length curve and surface unevenness (cloudiness) will be possible to amplify on relation between the *DR* function and surface unevenness. On the basis of course of individual curves, the level and the character of surface unevenness can be judged.

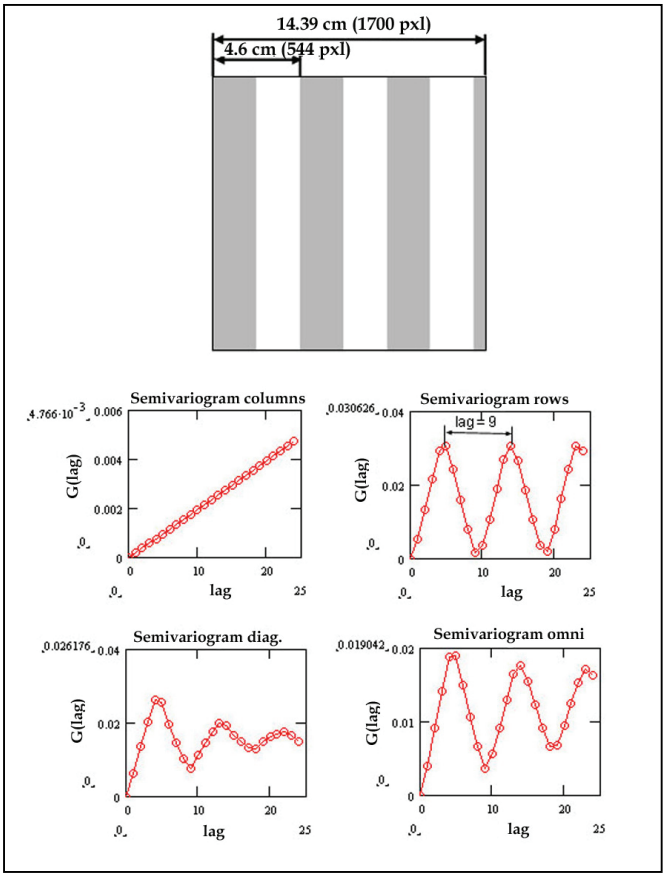

Fig. 22. Semivariograms from greyness degree of image – used whole image (1700 x 1700 pixels) without frame, step: 60 pixels

The surface unevenness of woven fabric can be evaluated by means of area variation curves and semivariograms of greyness degrees of fabric image. The area variation curve has been mentioned theoretically also in previous works (Wegener & Hoth, 1958); (Suh, 2005). From our experiment it has been found out that both the spectrogram and the variance-length curve of yarn used in fabric are basic indicators determining conceivable negative fabric appearance and this corresponding adverse course of area variation curve. Next indicator, which can be used in given context, is the *DR* function. The application of semivariograms has not been used by the other authors for the evaluation of surface unevenness of woven fabric yet. Semivariograms in the direction of both rows and columns seems to be a suitable tool for fabric stripiness evaluation.

Most of experiments have been done with fabrics (real or simulated images of fabric appearance) till this time. Thus, it would be interesting to verify obtained piece of knowledge on knitted fabrics. Next, it would be possible to find other functions suitable for the expression of unevenness of woven or knitted fabrics.

5. Acknowledgement

This work was supported by the project Textile Research Centre II No. 1M0553.

6. References

Březina, M.; Militký, J. (2002). Complex characterization of textile surface, *Robust'2002 – proceeding of twelfth winter school JČMF,* pp.50 –58, Hejnice, January 2002, Jednota českých matematiků a fyziků, Prague.

Cressie, N.A.C. (1993) *Statistics for spatial data*, J. Wiley, ISBN 0-473-00255-0, New York.

Militký, J.; Bajzik.V. (2000) : Description of thickness variation by fractal dimension, *Proceeding of 7th national conference Strutex*, pp. 165-170, ISBN 80-7083-668-7, Liberec, December 2000, Technical university of Liberec, Liberec.

Militký, J.; Rubnerová, J. & Klička, V. (2000). Spatial statistics and unevenness of surface mass of non-woven textiles, *Proceeding of 7th national conference Strutex*, pp. 199-203, ISBN 80-7083-668-7, Liberec, December 2000, Technical university of Liberec, Liberec.

Militký, J.; Klička, V. (2005). Characterization of textile mass variation in plane, *Proceeding of 5th world textile conference Autex 2005*, pp.750–755, ISBN 86-435-0709-1, Portorož, June 2005, University of Maribor, Faculty of Mechanical Engineering, Department of Textile, Maribor.

Moučková, E.; Jirásková, P. (2006): Area-variation curve of real woven fabric, *Proceedings of 13th international conference STRUTEX*, pp. 87-92, ISBN 80-7372-135-X, Liberec, November 2006, Technical University of Liberec, Liberec.

Moučková, E.; Jirásková, P. (2007): Influence of weft sett on course of area variation curve on woven fabric, *Proceedings of 6th international conference TEXSCI 2007, CD-rom edition,* ISBN 978-80-7372-207-4, Liberec, June 2007, Technical University of Liberec, Liberec.

Moučková, E.; Jirásková, P. (2008). Utilization of semivariogram for evaluation of surface unevenness, *Book of proceedings of 4th International Textile, Clothing & Design Conference – Magic World of Textiles*, pp. 848 – 853, 978-953-7105-26-6, Dubrovnik, October 2008, University of Zagreb, Faculty of Textile Technology, Zagreb.

Pinčáková, Z. (2006): Classification selected parameters and characteristic functions of mass irregularity, *Diploma Work* (Supervisor: Ursíny, P.), Technical University of Liberec, Liberec.

Slater, K. (1986). *Yarn evenness*, The Textile Institute, ISBN 0 900739 85 1, Manchester.

Suh, M., W. (2005). An electronic Imagining of Fabric Qualities by on-line yarn data, Available from www.ntcresearch.org/pdf-rtps/AnRp01/I01-A1.pdf Accessed: 2005-02-01.

Ursíny, P.; Moučková, E. & Jirásková, P. (2008). New knowledge about relation between yarn mass irregularity and surface unevenness. *Book of Proceedings of the 4th International Textile, Clothing & Design Conference - Magic World of Textiles*, pp. 915-920, ISBN 953-7105-92-, Dubrovnik, October 2008, University of Zagreb, Faculty of Textile Technology, Zagreb.

Wegener, W. & Hoth, E. G. (1958). Die CD(F)–Flächenvariation, *Textil–Praxis*, Vol. 1958, No. 13, (1958), 485- 488.

Zellweger Uster (1971). Zusammenhänge zwischen den Ergebnissen der Gleichmässigkeitsprüfung und den Aussehen der fertigen Gewebe und Gewirke. *Uster News Bulletin*, No. 15. (January 1971), 3 – 36.

Zellweger Uster (1988). Neue Möglichkeiten der Analyse von Masseschwankungen an Garnen, Vorgarnen und Bändern, *Uster News Bulletin*, No. 35. (August 1988), 6 - 18.

Zellweger Uster (2001). *Uster Tester IV Application Handbook*, V1.0/400 106-04010, Uster.

11

Detection of Defects in Fabric by Morphological Image Processing

Asit K. Datta[1] and Jayanta K. Chandra[2]
[1]*Department of Applied Optics and Photonics, University of Calcutta, Kolkata 700009*
[2]*Future Institute of Engineering and Management, Kolkata 700150*
India

1. Introduction

Defects are generated in woven fabric due to improper treatments in weaving machines, spinning errors and inadequate preparations of fiber at the spinning stage. The economic viability of a weaving plant is significantly influenced by the extent of its success in eliminating defects in fabric. Detection of defects is generally carried out by time consuming and tedious human inspection. Such manual inspection procedures are commonly agreed upon to be inefficient with detection efficiency suffering from deterioration due to boredom and lack of vigilance. The problem is accentuated by the presence of several types of defects those may occur in woven fabric at random.

In textile industry, imaging and image processing techniques are investigated for off-line and on-line visual inspection of fabric for the detection of defects (Zhang & Bresse, 1995; Drobino & Mechnio, 2006). The basic philosophy of detection of defects by such techniques is guided by the analysis of the image of fabric for distinguishing properties, those can be used to discriminate between defective and first quality fabric. In most cases, measurements are made on the first quality fabric and are then compared with the measurements made on the test fabric. Severe deviations in the measured parameters are used to indicate the presence of defects. Defects are then categorized into several types. However, the recognition of a particular type of defect amongst various classified types always remains a problem even in the context of presently available advanced image processing technology. Moreover, massive irregularities in periodic structures of woven fabric (particularly for fabrics manufactured from natural fibers) introduce very high degree of noise, which make identification and classification of defects difficult. The problem is accentuated very much due to the hairiness of natural fibers.

Elaborate image processing algorithms are usually adopted for detection and recognition of defects (Sakaguchi et al, 2001). Recent reviews are available on various techniques, those can be applied for such tasks (Xie, 2008). In this chapter we are interested to explore one of such techniques which can be termed as morphological image processing, for the detection of defects in woven fabric.

The techniques of morphological image processing are widely used for image analysis and have been a valuable tool in many computer vision applications, especially in the area of automated inspection (Haralick et al, 1987). Many successful machine vision algorithms used in character recognition, chromosome analysis and finger print classification are based

on morphological image processing techniques (Maragos, 1987). It has relevance to conditioning, labeling, grouping, extracting and matching operations on image (Dougherty, 1993). Thus, from low level to high-level computer vision, morphological techniques are important in operation such as noise removal and median filtering (Heijmans, 1994). Indeed many successful machine vision algorithms employed in industry, processing thousands of images are based on morphological techniques.

For the quality control in the textile industry, the technique of morphological image analysis has been used for assessing fiber composite material (Serra & Verchery, 1973) and carpet appearance (Xu et al, 1991) and texture analysis (Wermen & Peleg, 1985). Morphological image processing based technique has also been investigated for detection and classification of defects in fabric (Chetverikov & Hanbury, 2002). The morphological operations for defect detection in fabric are inherently sensitive to the size and shape of the defect. Therefore, while applying morphological image processing technique on the fabric image for the detection of defects, the software-based morphological operations may give poor result when the defects are relatively small in comparison to the fabric structure. The testing involves two stages of operations. First a structuring element is selected from the heuristic knowledge of the likely defects. Secondly, the test image is thresholded and then morphological operations are applied on the thresholded image of the test fabric for the identification of defects.

1.1 Types of commonly occurring defects in woven fabric

The defects in fabric are generally classified into three subdivisions according to the occurrence in the fabric. They are, (i) weft-way defects (ii) warp-way defects and (iii) defects with no directional dependence. There are about twenty-two types of defects usually associated with woven fabric due to various processing irregularities. Out of these twenty-two, only few are severe defects and need elimination by rejection at the production stages.

These severe defects are:

a. **Broken pick, short pick, double pick and pick' inhomogeneity**: These defects are sometimes referred to as mispick (float) or missing pick and result in a void in the fabric due to missing yarns. Sometimes, two adjacent threads with same interlacing are beaten up together as a result of broken picks. Double pick defect is mainly due to extraneous thread in the fabric.
b. **Slub (fly):** These defects usually appear in the fabric as abnormally thick places of varying length.
c. **Knot:** These defects usually appear in fabric as hardly discernible change in yarn thickness. Knots in fabric usually arise due to fastening of yarns.
d. **Snarl and snag**: A defect, where warp or weft yarns are twisted on itself and the loop is termed as snarl. A snag is produced when one or more pick is snagged on a knitted yarn.
e. **Reed mark (crack):** It is due to improper irregular interspacing of yarns and appears as a transparent strip.
f. **Thin place**: This defect arises out of insufficient density of yarns.

Apart from the above-mentioned major defects, mechanical defects such as hole piling, oil marks and other anomalies manifest themselves as defects in woven fabric.

In general, all defects alter the normal regular structure of fabric pattern and also modify the statistical and physical properties of the first quality fabric. The effects of defects are also dependent on the textural types of woven fabric.

2. Morphological image processing operations

Mathematical morphology is a tool for extracting image components that are useful in the representation and description of region shape (Serra, 1988). As a discipline within imaging, mathematical morphology concerns with the applications of its basic operators in all aspects of image processing. Conceptually, morphological operations are rooted in planar geometric structure which is altered by probing with a structuring element. Each operation uses the structuring element to determine the geometrical filtering process. satisfying four properties: translation invariance, antiextensivity, increasing monotonically and idempotence. The structuring element of a morphological operator is therefore a function defined in the domain of the spatial pattern. The value of each pixel of the domain is the weight or coefficient employed by the morphological operator at the pixel position.

The concepts of image processing using mathematical morphology were developed mainly as an application of set theory (Matheron, 1975; Serra 1988; Heijmans & Ronse 1990). The evolution of the theory closely follows the evolution and applications of pipeline and cellular computing techniques (Danielsson & Levialdi, 1981). By nineties many image-processing algorithms for morphological operations are evolved using electronic and optical techniques (Liu, 1989; Casasent, 1990; Botha et al, 1989; Mallick-Goswami & Datta, 2000). Optical morphological image processing was also applied for feature extraction and shape description (Gracia et.al, 1993).

The morphological image processing technique has its roots in texture analysis and in the problems of determining properties of the texture. Its underlying idea is to use a so-called structuring element to define neighbourhood of points in an image. Operations with the structuring element may smooth the contours of the objects or may decompose an image into its fundamental geometrical shapes. Morphological operations can be applied not only on binary image but also on gray level images (Vincent, 1993).

Fundamental morphological operations are erosion and dilation. These operations remove or add pixels from a binary image according to rules that depend on the pattern of the neighboring pixels. The erosion operation reduces the size of an image, while the dilation operation enlarges geometrical size the image. Two other derived morphological operations are opening and closing. An opening is an erosion operation followed by dilation, and a closing operation is a dilation followed by an erosion operation. Each of these operations uses the structuring element to determine the geometrical filtering process.

In morphological operations, the choice of structuring element is very critical and is generally guided by apriori knowledge of processing tasks. However, there are several studies, where the selection of structuring element is guided by a training phase for a particular situation (Camps el al, 1996).

2.1 Binary morphological image processing operations

We restrict ourselves to the specific case of a gray fabric image $F:Z \to \bar{R}$ defined on a sub-section of the two-dimensional Euclidean space R^2. The notation $\bar{R}$ indicates the set R∪{-

$\infty,+\infty\}$. In other words, the function assigns a grey-level to each point $x \in Z$ of the fabric image. In practice, however, the Euclidean space is replaced by a discrete space Z^2. The gray values taken by F are often limited to integers and the pixel value at position x is denoted by F(x). For 8 bit gray scale images, $F(x):Z \rightarrow \{0.1.2\ldots\ldots\ldots\ldots\ldots,255\}$.
The morphological operations are defined as set operations and can be applied for processing of fabric images by defining another selected image *S* called structuring element. Therefore S is a subset in the two dimension Euclidean space. S can be a binary image or a gray image. The classical Minkowsky set addition and subtraction of these two images F and S are defined in set notation as,

$$\text{Addition:} F \oplus S = \{x+a : x \in F, a \in S\} = \cup F_a \big|_{a \in s} = \cup S_a \big|_{F \in S} \tag{1}$$

$$\text{Subtraction} : F \Theta S = \bigcap F_a \big|_{a \in s} \tag{2}$$

where F_{-a} is the translate of the image set along a and is defined as,

$$F_a = \{ F + a : x \in F\} \tag{3}$$

The transformation $F \rightarrow F \oplus S$ and $F \rightarrow F \Theta S$ are called a dilation and erosion operation by structuring element S. According to standard convention the morphological dilation operation on the image F by the structuring element image S is given by,

$$\text{Dilation:} F \oplus \bar{S} = \left\{ h \in E : \left(\bar{S}\right) h \cap \frac{F}{\varphi} \right\} \tag{4}$$

$$\text{Erosion:} F \Theta \bar{S} = \{ h \in E : S_h \subseteq F \} \tag{5}$$

where h is an element in Euclidean space and, φ denotes the empty set.
The reflected or the symmetric set $\bar{S}$ is related to S by the following equation,

$$S = \{ -a : a \in S\} \tag{6}$$

Self complementation of the set yields a duality relation and the dilation operation is also expressed as:

$$F \oplus \bar{S} = \left(F^C \Theta \bar{S} \right)^C \tag{7}$$

where, F^C is the complement of the set constituting the image F.
By definition, morphological opening is erosion followed by dilation and the closing operation is viewed as the complimentary process of opening. Therefore, the opening and closing operation are denoted in set notation as,

$$\text{Open} : (F,S) = \left(F \Theta \bar{S} \right) \oplus \bar{S} \tag{8}$$

$$\text{Close} : (F,S) = \left(F \oplus \bar{S} \right) \Theta \bar{S} \tag{9}$$

The opening is the union of all translates of the structuring element that is included in the set F. It may be noted that both opening and closing operations are translation invariant. Opening and closing are related to Boolean duality by,

$$\text{Close: } (F, \bar{S}) = \text{open} : (F^c, S)^c \tag{10}$$

2.2 Gray morphological image processing operations

Binary morphological operations are performed for the sets whose elements are vectors corresponding to pixel positions and therefore are *set-set operations*. A grayscale image can be considered as a three-dimensional set where the first two elements are the x and y coordinates of a pixel and the third element is the gray-scale value. The key issue is to use the infima/suprema (minima and maxima in discrete cases) to define gray-scale morphological operators (Chu-Song et al. 1999; Heijmans 1999). The structuring elements of the gray-scale morphological operations could have the same domains as those in binary morphology. However, a gray-scale structuring element is also possible having certain values instead of having only value 1 or 0. Therefore, morphological operation of gray scale images with binary structuring element is a function-set operations and the operation for gray images and gray structuring element are function-function operations (Sternberg, 1986). The pixel value of a gray fabric image F at position x is expressed by a function f(x). The gray scale erosion and dilation with as binary structuring element *S* can then be defined as,

$$\text{Function set erosion: } \left[f \Theta \bar{S}\right](x) = \inf_{x \in S_x} f(x) \tag{11a}$$

$$\text{Function set dilation: } \left[f \Theta \bar{S}\right](x) = \sup_{x \in S_x} f(x) \tag{11b}$$

However, in case of operations with gray scale structuring element g^S, the gray morphological operations are defined as,

$$\text{Function} - \text{function} - \text{erosion: } [f \oplus g^S](x) = \max_{y \in G} \{f(x+y) + g(y) \tag{12a}$$

$$\text{Function} - \text{function} - \text{dilation} : [f \Theta g^S](x) = \min_{y \in G} \{f(x+y) g(y)\} \tag{12b}$$

Gray-scale opening and closing are defined in a similar manner as the binary case. The only difference is, when the operations are carried out, these opening and closing operations use gray-scale dilation and erosion. As binary morphological operations do, gray-scale opening is anti-extensive and gray-scale closing is extensive. Both operations make an original image smooth along to the nature of minimum and maximum functions.

3. Morphological operations on image of fabric

It is evident that F is the image of test fabric and *S* is the image of structuring element, which in most of the cases is a binary image. Selection of structuring element image is important in morphological image processing for defect detection in fabric. A particular defect in the fabric image can be detected by eroding the image with a structuring element that is slightly

smaller than the shape of the defect. For example, if the dimension of the structuring element is made slightly smaller than the average dimension of a knot, then the erosion operation of the fabric image with the structuring element will result in the complete elimination of the weft and warp structure. However, the selection of structuring element is not easy for the detection of thick yarn as the yarn may run through out the entire length of the fabric.

While applying the binary morphological image processing operations as defined, it is necessary to obtain binary image of the fabric. Segmenting the gray level pixel values of fabric image into two gray level values are all that is required to produce a binary image of fabric. Let, I(i, j) is the gray level pixel value at point (i,j) of the input fabric image and F(i,j) is the gray level of point (i,j) of the output fabric image. The binary image is obtained from the gray level image by converting the pixel value to 1 (white pixel) if the value is greater than the preselected threshold value: otherwise the pixel value is returned to 0 (black pixel). It is assumed that the threshold value does not depend on the spatial coordinates (i, j) and also threshold value is independent of local properties of the point.

3.1 Extracting defects from image of fabric

Detection of defects by morphological operators are carried out for few test samples of woven fabric. For example, three types of typical defects such as a knot (fig. 1a), thick weft (fig.1b) and missing weft (fig. 1c) are subjected to morphological operations with a 3×3 structuring element. Since the fabric images are gray images, gray to binary image conversion by thresholding is necessary for defect detection. The thresholded binary images are shown in figures 1d, 1e and 1f. The morphological erosion and opening operations on the thresholded images are shown in set of figures 1g, 1h and 1i and figures 1j, 1k and 1l. It has been observed that a rectangular structuring element of 3×3 pixel size is sufficient for extracting the defects such as knot from the test fabric either by erosion of by opening operations. However, in case of detection of thick weft by opening operation is not very efficient though the detection is better than erosion operation. The detection of missing weft by erosion and opening operations needs higher size structuring element. A 5×5 rectangular structuring element gaves better results than using a 3×3 structuring element. This is because of the continuity of the defective yarn throughout the length / breadth of the test fabric.

From the results, it is shown that the presence of knot and thick yarns are detected more clearly by the erosion operation than the by opening operation. However for opening operation a structuring element of 5×5 is used. The detection of missing weft by erosion and by opening operations, however, is hopelessly useless even by using structuring elements of higher areas.

3.2 Morphological operations by removal of interlaced grating structure of fabric

While detecting defects of various sizes in test fabrics, the results of morphological operations are much better, if the basic grating structure of the fabric due to weft and warp interlacing is removed by spatial filtering. To accentuate the gray values of the pixel positions of defects and to properly distinguish them from the cross-points, it is necessary to process the fabric image with a view to smooth out or remove the cross points. The processing is done by optical or digital spatial filtering of the de-noised image F_{dn} to yield the spatial filtered image F_{sf}. A binary fabric image F_b can then be obtained from the spatial

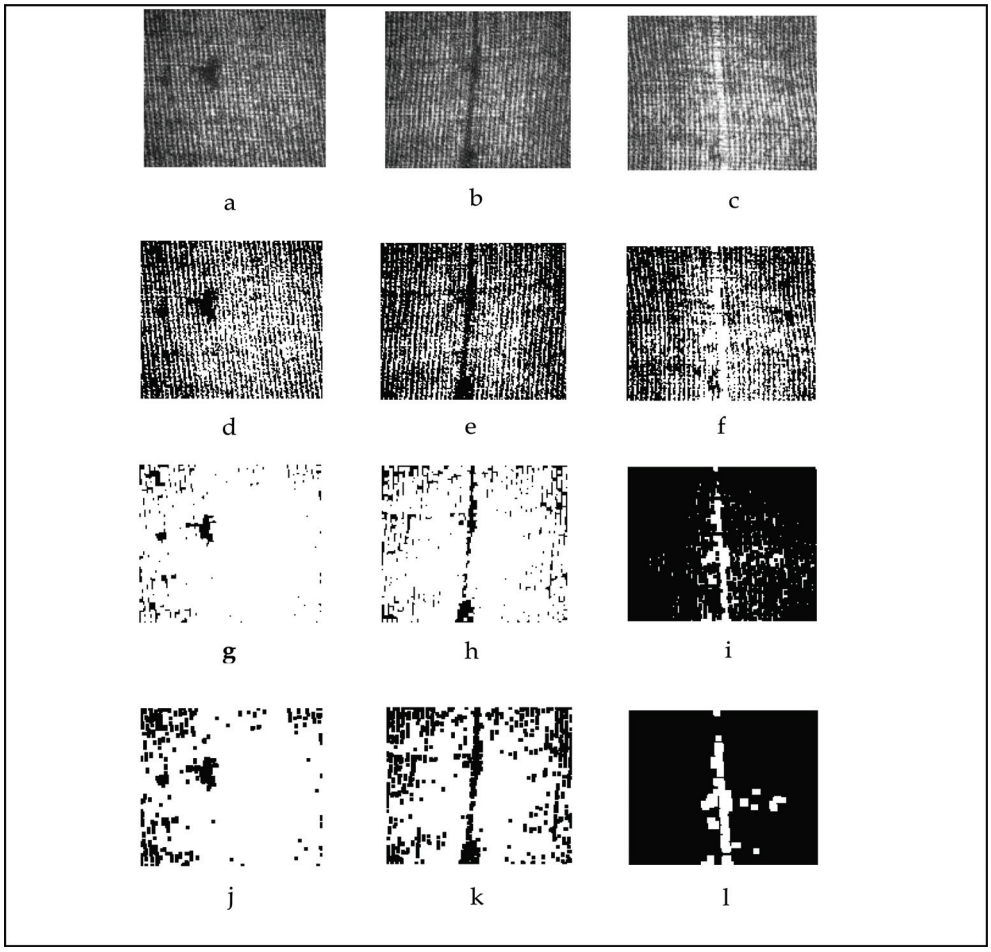

Fig. 1. Test fabrics with defects (row 1), thresholded images (row 2) and results of defect detection by morphological erosion (row 3) and opening operations (row 4).

filtered image, when the pixels are converted to either 1 or 0, if it is above or below a pre-selected threshold value P_{th}. Therefore, F_b=1, if F_{fs}>P_{th} and F_b=0 if F_{sf}<P_{th}. The threshold value P_{th} is however, depended on the type of fabric.

The test results of morphological operations after the removal of grating structures of fine, medium and coarse fabric are shown in Fig. 2. Some general conclusions can be drawn from the results. It is not possible to remove the grating structure of warp and weft yarns by digital spatial filterig, particularly for coarse fabric when the size of defects are comparable or slightly bigger than the yarn diameter (row 2 of fig. 2). In fine and medium fabrics, it is possible to remove the interlaces grating completely by suitably selecting the diameter of spatial filter and the threshold value. For defect detection opening, dilation, erosion and closing operations are performed. The type of morphological operations to be performed depends on the types of defects present in the test fabric. The result follows the expected

pattern for long defects, since the connectivity of the yarn in the whole image set is higher than that of the defects. In fig. 2, for the detection of defect present in the first type of test fabric opening operations are carried out. For defects in the second, third and fourth types, dialtion, erosion and opening operations are carried out respectively.

4. Morphological filtering operations for noise removal from fabric image

Before applying the morphological operations for the detection of defects in woven fabric, the gray fabric image F is *de-noised* by using morphological filtering technique. This preprocessing is necessary particularly for cotton fabric, where the presence of hairiness is more likely to occur. Since noise in an image should be removed wherever it is located, the translation invariance property of filter is required for noise removal. Translation invariant operations are justifiable also for a fabric image where noise in the image is dimensionally

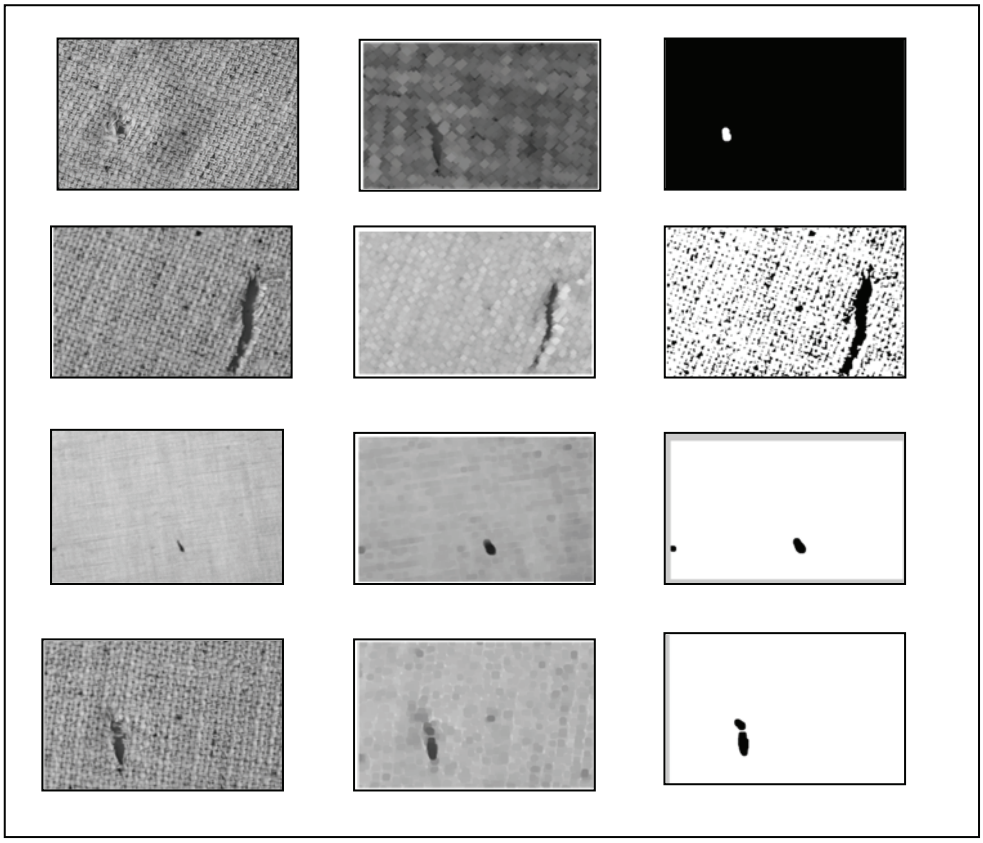

Fig. 2. Test results of morphological operations after removal of interlaced grating structure. Column 1 shows the images of test fabrics, column 2 shows the spatially filtered images of column 1. Column 3 shows the detection of defects by morphological operations on images of column 2.

smaller than the defects. The morphological filter, which can be constructed on the basis of the underlying morphological operations, are more suitable for noise removal than the standard linear filters since the latter sometimes distort the underlying geometric form of the image (Maragos & Schafer, 1987). Therefore, these filters are more suitable for noise removal (Podaru & Stanomir, 2003).

The morphological filtering is restricted to all image-image transformations that are translation invariant and increasing idempotent operations characterized by $\varphi[\varphi(F)]=\varphi(F)$, where φ is an operation. The filter $\varphi(F)$ is decomposed into OR operation of erosions by a structuring element S and is expressed as,

$$\varphi(F)=\bigcup_{S\in\ker[\varphi]} F\Theta\bar{S} \tag{13}$$

where F is a fabric image and ker[φ] is the kernel of φ given by, $\ker[\varphi]=\{F \mid 0\in\varphi(F)\}$.

Extensivity and anti-extensivity of the operations are not always useful for practical situation of noise removal. Since median filter is not extensive or anti-extensive, but handles white objects and black backgrounds equivalently, morphological representation of median filter is very useful for de-noising. The cascades of opening and closing with an elementary (2×2) binary structuring element S is used for this purpose. Since the structuring element is symmetric, reflection of S is the S itself. The de-noised image F_{dn} is obtained from gray fabric image F by the following processing steps:

$$\text{open}(F)=(F\Theta S)\oplus S) \tag{14}$$

$$F_{dn}=\text{close}[\text{open}(F)]=([\text{open}(F)]\oplus S)\Theta S \tag{15}$$

By this process most of the noise present in the fabric image is removed while maintaining the shape and size of the defects almost intact.

5. Rank order operator: generalized morphological operations

The detection of small defects such as knots and broken picks in woven fabric is difficult because of the presence of confused background due to the interlaced periodic structure of the warp and weft, which result a large number of almost regular crossover points. Moreover, hairiness of the fabric introduces high dose of noise into the image pattern of the fabric.

In the Section 3, it has been shown that the morphological erosion operation can erode the grating structure of the fabric to a certain extent and might be suitable for the identification of defects. However, complete erosion of the background is not possible unless very judicious choice of the structuring element is made. For detection of defects of small size in woven fabric, simple morphological erosion operation with a comparatively large structuring element is not efficient. In such cases, there are always chances of complete erosion of the image. Dilation also may cause the entire cross point background of the image to fill in resulting in a completely dark search space (background). In many cases, there is a need to erode first by a small structuring element and then apply a larger one. This may somewhat solve the problem, however this is not always possible, particularly for the detection of defects in fabric where the failure rate of such a solution is frustratingly high.

It is shown in this section, that the binary rank order operation (Heygster, 1980; Arce & Foster, 1989) gives satisfactory result when the expected size of defect is considered in

selecting of structuring element. Moreover, the rank order operator has unique property of image smoothing and presenting edges and at the same time it is very efficient for noise removal. In a woven fabric, repetition of the interlaced grating structure is not very accurate and therefore rank order operation proves to be an efficient tool for defect detection.
It may be noted that the rank-order operator is a generalization of the morphological erosion and dilation operations. Erosions and dilations are convolutions with maximum and minimum threshold value respectively. Therefore rank order operations require a structuring element as well. Rank order operator rotates in planar geometric structure, which is altered by probing with a structuring element called reference image. Each operation uses the reference image to determine the geometrical filtering process. The reference image or the structuring element of the operator is therefore a function defined in the domain of the spatial pattern of the operator.

5.1 Binary convolution operation

The rank order operation can be performed by a linear convolution between input image and reference image (structuring element image) followed by thresholding of the convolution output. Simplest image convolution operation of image is a process that copies one image at each pixel location of another while allowing for the effects of all pixel values in the area where the copy takes place. A multiplying, adding and shifting operation accomplish this. A convolution c(p) of a binary fabric image F(u) by structuring element S(u) is given by,

$$c(p) = \sum_{u} F(p-u)S(u) = F * S \tag{16}$$

where, p and u are two-dimensional spatial vectors, $u,p \in Z^2$, and the summation is over the Z domain of the image.

5.2 Binary nonlinear rank order filter

In recent years, several rank-order structuring filters are proposed. These filters are roughly divided into two categories. The set of adaptive rank-order filters fall under the first category (Lee & Fam, 1987), while the second class encompasses structure preserving rank-order filters (Niemnien et al, 1987). Adaptive rank-order filters are used on images with low signal-to-noise ratios and some a priory knowledge or local statistics are required for processing (Stevenson & Arce, 1987). The main advantage of the non-adaptive type lies in the fact that the extensive use of local statistics is not necessary.
The rank order filter while applied on binary image is also called an order statistic filter or a a Ξ filter (Preston, 1983). A binary rank order operations can be replaced by operations of counting the number of image points that contacts the points of the structuring element probe and marks the reference point in the output image if at least a given percentage of points contact the probe. The percent point or the threshold is a variable and is adjusted for good performance in a particular application.
Widely employed nonlinear and locally adoptive filters are rank order filters. The threshold operation X_t is applied to eq.16, at threshold t, to get the output result after rank order filter operation and is given by,

$$R_t(F,S)(p) = X_t\left(\sum F(p-u)S(u)\right) = X_t(F * S) \tag{17}$$

For a rank order operator R_t expressed in this from, threshold t is the rank. The threshold operation X_t is performed under the conditions that,

$$\begin{aligned} X_t &= 1 \quad \text{if} \quad c(p) \geq t \\ &= 0 \quad \text{otherwise} \end{aligned} \tag{18}$$

5.3 Choice of the proper rank of the rank order operator

Two problems are encountered while applying the rank order operator for defect detection in fabric. They are related to the (a) choice of reference image (i.e. structuring element) and (b) the choice of the rank. The value of each pixel of the domain is the weight or coefficient employed by the pixel position. The selection of the size and shape of the reference image is hence an important step for defect detection. When the size of the reference image is almost same to the size of the defect to be detected the most efficient and optimum detection capability is expected. Evidently the size of the domain can be ascertained from priory knowledge of the likely defect in woven fabric.

The rank selection is based on the boundary characteristics. One of the most important aspects in selecting a rank is the capability of reliably identifying the mode peaks in a given image histogram. This is particularly important for automatic threshold selection in situations where image characteristics can change over a broad range of intensity distributions as in the case of woven fabric. Therefore the rank of the operator has to be decided also from a priori knowledge of the periodicity of the fabric structure and the diameters of the warp and weft yarns.

The rank of a particular operation is a function of the reference image or the structuring element S and the intensity values of the test fabric F. A simple relation is established between the rank R and the dimension D of the structuring element S and the maximum value M of the convoluted matrices for quick selection of a rank for a particular operation. The relation is given by,

$$R=255(k)(D)-M \tag{19}$$

where, k is a positive low value and M is obtained by dilation operation as $M=\max(F \oplus S)$.

If F (the test fabric) is a $(m \times n)$ matrix and if S (the structuring element or the reference image) is a $(m_1 \times n_1)$ matrix, then the convoluted matrix has dimension $(m \times n) \times (m_1 \times n_1)$. So the dimension of the output matrix increases correspondingly. The conversion of $(m \times n) \times (m_1 \times n_1)$ matrix to $(m \times n)$ output matrix eliminates the data outside the region of interest.

5.4 Defect detection of fabric by rank order operator

Fig. 3 shows the presence of a knot, oil mark and thick yarns respectively, as defects in the test fabrics. A structuring element of size 15 X 15 is used for rank order filtering of the basic grating structure of the fabric at the value of k = 0.657.

It is seen that the knot is extracted efficiently (fig. 3, first column). In contrast to the erosion operation (Fig 2), the size of the knot is not reduced and is maintained in the detection process of the rank order filtering. The oilmark is also detected as defect by the same process (fig. 3, second column). The detection of thick yarns in the test image of fig. 3 is shown in third column. A scrutiny of fig. 3f will shows the existence of not only a thick weft at the

bottom but also the existence of a slightly thicker yarn (weft) on the upper portion of the fabric. Also existence of the defect of slightly thicker yarn escapes visual inspection and the can not be detected by morphological operations described in sections 3 and 4. However, by selecting an elongated structuring element 4 X 132 and the value of k = 0.657 (which matches closely the diameter of the yarn) and the defect is detected by rank order filtering.

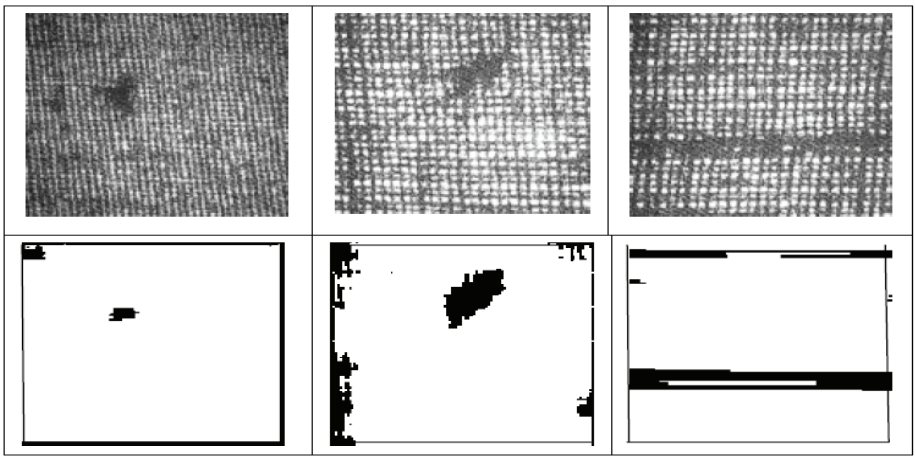

Fig. 3. Shows the presence of defects, knot, oilmark and thick yarns (top row). The bottom row shows the detection process by rank order filtering.

6. Selection of the size structuring element by artificial neural network

Selection of structuring element in all morphological operations is one of the major problems while detecting defects in woven fabric. The size and shape of structuring element has to be different for different textures of fabric and also has to be different for identification of different types of defects. In general, the selection of structuring element is done heuristically or by trial and error basis. In order to overcome the problem of selection of the size of the structuring element, decomposition of the structuring element is proposed (Park & Chin, 1995; Roerdink & Heijimans, 1988). One can also process (e.g., extract or eliminate) differently scaled objects of interest in the image by adapting the size of the structuring element(s) to the local intensity range (Masayasu, Masayoshi, & Akira, 2003). Attempt has been made to use optimally selected structuring element (Schonfeld, 1994) and optimal selection is applied for the defect detections in fabric (Mak, Peng, & Lau, 2005). Since biological neurons can adopt itself to a new situation and can be trained, the selection of structuring element can be done by training from the image data to be processed for a specific application. Any simple artificial neural network model may be useful for training (Lippman, 1989). However, particularly defect detection problems where association of a single class is required for many disjoint regions in the pattern space, a multi layer perceptron (MLP) model with a hidden layer of neurons is necessary (Widro, & Lehr, 1990).
The signal flow in a MLP model is shown in Fig. 4, where w denotes the weight, I and O are the input and output signals with proper subscripts h and o for hidden and output layer. The hidden layer neurons generate hyper planes that are building blocks of decision

regions. In MLP architecture, linear threshold unit is used for generating activation function form input layer neurons to the hidden layer neurons and sigmoidal threshold function S[.] is required for generating activation functions from hidden to output layer neurons. A real parameter λ determines the sigmoidal activation gain. Each neuron of the input layer is connected to each neuron of the hidden layer after being multiplied by the weight vectors and similarly each neuron of the hidden layer is also connected to each neuron of the output layer after being multiplied by the weight vectors. During the training process, up-gradation of the weight vectors takes place and continues till an error term ε goes below a certain predefined tolerance value. A learning rate coefficient η determines the size of the weight adjustments made at each iterations and hence influences the rate of convergence. The learning rate has to be kept small in order to maintain smooth trajectory in weight space. Large learning rate leads to oscillations during learning and it is necessary to introduce a momentum term α into weight update procedure. Many algorithms exist for training and testing in MLP model (Haykin, 2008).

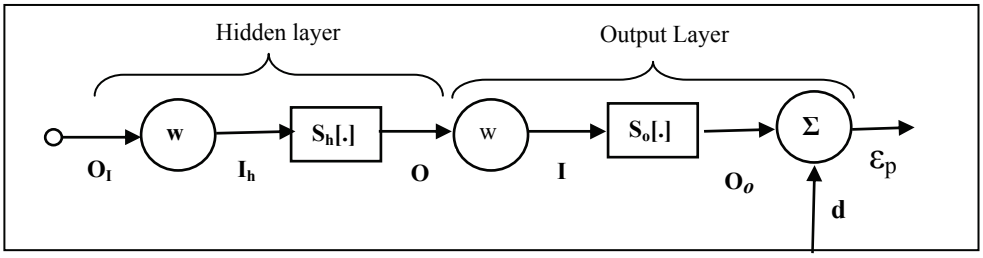

Fig. 4. Signal flow in artificial neural network model

If (u x v) is the size of the structuring element needed for the morphological operation, then this parameter should relate to the fabric parameters for training the ANN. For this purpose each sample of fabric is assigned a set of two normalized numbers Z_1 and Z_2 for their identification. Z_1 is a normalized number related to threads per centimeter of fabric along the weft direction (say *x*-axis) divided by an integer number (say N, where N>1), so that Z_1 can be expressed as a fraction. Similarly, Z_2 is a normalized number related to number of threads per centimeter of the fabric along warp direction (say y-axis). Z_2 is also expressed as a fraction by dividing by N. Given a training set vector pairs of fabric parameters Z_1 and Z_2 for P different types of fabrics, the network is trained for different types of defects to yield trained size of structuring element required for morphological operation.

7. Conclusion

It has been shown in this chapter that morphological operations can be exploited for detection of various types of defects in the woven fabric. However, the erosion operation on fabric image helps in detecting defects to a major extent. Binarization of the fabric image is necessary before applying the morphological opeartions. The detection capability improves if the image is spatially filtered and then thresholded to remove the interlaced grating structure of the fabric. Moreover, gray morphological operations is possible for the defect detection and more accurate detection is possible than the binary morphological processing. In this chapter it is alos shown that detection capability is greatly improved by rank-order filtering which is termed as generalized morphological operations. The method offers two

flexible controls. The structural element can be selected according to *a priori* knowledge of the defect. Secondly, the rank can be selected to suit a particular noisy situation. It has been established that very good detection is possible for small size defects (such as a knot) in all types of fabric by rank order filtering technique.
Proper selection of the structuring element in all morphological operations enhances the chance of detection of defects which otherwise may not be very distinct even during visual inspection. A method has been shown where the size of the structuring element can be selected as a result of training of the system by artificial neural network.

8. References

Arce, G. R.; & Foster, R. E. (1989). Detail preserving ranked order based filters for image processing, *IEEE, Trans, Acou. Speech & Sig. Processing*, Vol. 37, No 1, 83-89.

Botha, E.; Richards, J.; & Casasent, D. (1989). Optical laboratory morphological inspection processor, *Applied Optics*. Vol 24, No 11, 5342-6.

Camps, O.I.; Kanungo, T.; Haralick, R. L. (1996). Grey-scale structuring element decomposition. *IEEE Trans. Image Processing.,* 5, 111-120.

Casasent, D. (1990). Optical morphological processors, *Proc. SPIE*, Vol. 1350, p 380-384.

Chetverikov, D; Hanbury, A., (2002). Finding defects in texture using regularity and local orientation,. *Pattern Recognition,* 35,10-15.

Chu-Song, C; Ja-Ling, W.; Yi-Ping, H. (1999). Theoretical Aspects of Vertically Invariant Gray-Level Morphological Operators and Their Application on Adaptive Signal and Image Filtering, *IEEE Trans. on Signal Processing.*, 47, 4, 1049-53

Danielsson, P. E.; & Levialdi, S. (1981) Computer architectures for pictorial image information systems. *IEEE computer Magazine.* No 11, 53-58.

Drobino, R.; & Machnio, M. S. (2006). Application of image analysis technique for textile identification. *AUTEX Research J.* 6,1, 40-48.

Gracia, J.; Szoplik, T. & Ferreira, C. (1993). Optoelectronic morphological image processor. Optics Letter. Vol 17, No 10, 1952-60.

Haykin, S.,(2008) *Neural Networks,* Delhi, Pearson Prentice Hall.

Haralick, R.; Sternberg, S. & Zhuang, X. (1987). Image analysis using mathematical morphology. (1987). *IEEE Trans Pattern Analysis and Machine Intelligence.* Vol 9, no 4, 532.

Heijmans, H. J. A. M.; (1994) *Morphological image operators*" Academic , Boston.

Heijmans, H. J. A. M.; & Ronse, C. (1990). The algebraic basis of mathematical morphology - I: Dilations and erosions, *Comput. Vis., Graph., Image Process.: Image Understand.*, 50, 245–295.

Heijmans, H. J. A. M. (1999). Connected morphological operators for binary images, *Comp. Vis. and Image Understan.*, 73, 99–120.

Heygester, H. (1980). Rank filters in digital image processing. *Proc. 5th Int. Conf. on pattern Recognition, Florida*, 1165.

Lee. Y. H. & Fam, A. T. (1987). An edge gradient enhancing adaptive order statistic filter. *IEEE, Trans, Acou. Speech & Sig. Processing,* Vol. 35, No 5, 83-9.

Liu, L. (1989). Optoelectronic implementation of mathematical morphology. *Optics Letter*. Vol. 14, 482-88.

Lippmann.,R.P.,(1989). Pattern classification using neural networks. *IEEE Communication Magagine.* 2747-64.

Mak, K.L., Peng, P., & Lau, H.Y.K., (2005). Optimal morphological filter design for fabric defect detection, *IEEE International Conference on Industrial Technology*. 14-17 Dec. 799 – 804.

Masayasu, I., Masayoshi, T., & Akira, N. (2003). Morphological operations by locally variable structuring elements and their applications to region extraction. *Ultrasound images, System and Computation*, ,34, 98-103

Mallik-Goswami, B. & Datta A. K. (2000). Detecting Defects in Fabric With Laser- Based Morphological Image Processing, *Tex. Res.J.*, 70, 758-762.

Maragos, P. & Schafer, R. W. (1987). Morphological Filters- Part I: Their Set- Theoretic Analysis and Relations to Linear Shift-Invariant Filters, *IEEE Trans. Acoust., Speech, Signal Processing.* 35, 8, 1153-1169.

Maragos, P. & Schafer, R. W. (1987). Morphological Filters- Part II: Their Relations to Matheron, G. (1987). *Random sets and integral geometry*, Wiley, N. Y. 1975Median, Order-Statistic, and Stack Filters, *IEEE Trans. Acoust., Speech, Signal Processing,* 35, 8, 35. 8. 1170-1184.

Maragos, P. (1987) Tutorial on advances in morphological image processing, Opt. Engg. vol26, no3, , 623-28.

Nieminen, P. Heinonen and Y. Neuvo, (1987). A new class of detail-preserving filters for image processing, *IEEE Trans Pattern Anal. Machine Intelli.*, Vol 9, No. 1.

Park, H., & Chin. R.T., (1995), Decomposition of arbitrarily shaped morphological structuring elements. *IEEE Trans. Pattern Analysis & Machine Intelligence*, 17, 2-15.

Podaru, E.; & Stanomir, D. (2003) Noise suppression using morphological filters, *Proc. Int. Symp. Signals, Circuits, Systems,* 1, 61–64.

Preston, K. (1983). Ξ Filters. *IEEE, Trans, Acou. Speech & Sig. Processing*, Vol. 31, No 4.

Rumelhart, D.E., Hinton, G.E., & Williams., R.J. (1986). Learning representation by back propagating errors. *Nature.* 323, 533-36.

Roerdink, B.T.M., & Heijmans. H.J.A.M, (1988), Mathematical morphology for structuring elements without translation symmetry, *Signal Processing.*, 15, 271–277.

Schonfeld, D. (1994), Optimal structuring elements for the morphological pattern restoration of binary images, *IEEE Trans. Pattern Analysis & Machine Intelligence* 16, 6, 589–601.

Sakaguchi., Hua-Wen Guang. Matsumoto, Y. Toriumi., K & Hyungsup, K. (2001). Image Analysis of Woven Fabric Surface Irregularity , *Tex. Res. J.* 71, 666-67.

Serra, J. & Verchery, G. (1973). Mathematical morphology applied to fiber composite material, *Film. Sc. Tech.* Vol 6, No 1, 141-49.

Serra, J. (1988). *Image analysis and mathematical morphology*, Academic press, London.

Stevenson, R. L. & Arce, (1987). G. R. Morphological filters: Statistics and further syntactical properties. *IEEE Trans. Circuits & system*, Vol 34. No 11.

Sternberg, S. R. (1986). Grayscale morphology. *Comp. Vision, Graphics and Image Processing,* Vol. 29 no3.

Vincent, L. (1993). Morphological Grayscale Reconstruction in Image Analysis: Applications and Efficient Algorithms, *IEEE Trans. on Image Processimg*., 2, 2, 176-187.

Wermen, M. & Peleg, S. (1985). Min-max operators in texture analysis, *IEEE Trans. Pattern anal. Mach. Intelli.* Vol 7, No6, 730-36.

Widrow, B. and Lehr, M.A., (1990) 30 years of adaptive neural networks: perceptron, Madaline and backpropagation, *Proc. IEEE*, 78, 9 1415-1442.

Xie, X. (2008). A review of recent advances in surface defect detection using texture analysis techniques. *Elect. Letters on Computer Vision and Image Analysis*, 7, 3. 1-22.

Xu, B. Pourdeyhemi, S & Spivak, M. (1991). Texture evaluation of carpets using image analysis, *Textile Res. J.* Vol 60, No 3, 407-16.

Zhang. Y. F. & Bresee, R. R. (1995). Fabric defect detection and classification using image analysis. *Textile Res. J.* Vol 65, No 1, 1-10.

12

Investigation of Wear and Surface Roughness of Different Woven Glass Fabrics and Aramid Fibre-Reinforced Composites

Haşim Pihtili
Firat University, Engineering Faculty, Department of Mechanical Engineering, 23279 Elazığ
Turkey

1. Introduction

Composite Materials with Plastic Matrix has attained a broad utilization area due to their several qualities such as lightness, rigidity, heat resistance, high endurance limit, good resistance to wear in space and aircraft industry, automobile industry (piston, parts of engine, fan and compressor), sports and sea materials. Although manufacturing industry has developed good methods of manufacturing with modern machining, the traditional hole drilling method is still the most commonly used operation process due to its being economical and simple applicability. Drilling process is quite commonly used in defense, aviation and automobile industries [1]. In the production industry, non-metal composite materials are just beginning to be used alternatively instead of steel and other metals. Polymers and their composites are being increasingly employed in view of their high strengths and low densities. Many studies reported that the wear resistance with polymer sliding against steel improved when the polymers are reinforced with glass or aramid fibres. However, the behaviour is affected by factors, such as the type, amount, size, shape and orientation of the fibres, the matrix composition and the test conditions, such as load, speed and temperature [2.3.4–5]. The wear resistance of materials is determined by experiments that carefully performed in the laboratory.

Drilling process is quite commonly used in defence, aviation and automobile industries. When studies regarding processing composites are examined, we encounter commenly the composites with metal matrixes. In general in drilling tests made on metal matrix composites (MMC), it is seen that team wear is more and surface roughness is weak when classical high speed steel drills are used [6].

In this study, the effects of progress speed, rotation number, drill type and drill diameter on surface roughness of work sample are investigated while composite material is being machined by drilling. Besides, the wear behaviour of two woven glass fabric, namely the 300 and 500 grades, as well as aramid fibre-reinforced composite materials are investigated under different loads, speeds and sliding distances.

HSS, TIN and Carbide drills with 5, 10 and 15mm diameter were used in drilling processes. Experiments were performed with dry drilling by using values of cutting speeds of 125, 250 and 315 rpm and progresses of 0.056, 0.112 and 0.16 mm/rev.

2. Materials and specimens

In this study, woven glass fabric-reinforced composites, made of 300 and 500 gm^{-2} plain weave glass fabric, contain E glass fibres of diameter 10–24 μm were used. The woven glass fabrics are woven in two perpendicular directions. The woven glass fabrics composites consist of fibre, V_f = 30 vol.%, and matrix, V_m = 70 vol.%. Polyester resin was used as the matrix material for both composites. Another used specimen was the aramid fibre-reinforced composite. It has aramid fibres with a diameter of 10–24 μm. The aramid fibre-reinforced composite consists of fibre, V_f = 60 vol.% and matrix V_m = 40 vol.%. Epoxy resin was used as matrix material. The aramid fibre reinforced composite has been made by using filament winding process. There are three winds in this composite. The wind angle is equal to 45^o. This method produces very strong composites; therefore extremely large cylindrical and spherical vessels can be built [7]. Automotive drive shafts, helicopter blades, oxygen tanks are among the applications of filament winding [8]. All composite specimens were cut in size of 47mm × 27mm for wear tests. The woven glass fabrics and aramid fibre-reinforced composites have 4 and 1.5mm thickness, respectively.

3. Wear tests

The wear tests were performed by using a block-on-shaft test method (Fig. 1). 15mm diameter ground shaft, SAE 1030 (DIN 22) steel, was used as the counterbody. The hardness and surface roughness (*R*a) of the shaft were 150 HB30 and 1.25 μm, respectively. The wear tests were performed on a specially prepared experimental set-up by using a lathe. The actual loads were placed on the pan of the load arm of this apparatus. The schematic view of wear set-up is shown in Fig. 1. All the experiments were conducted at room temperature. The temperature of the specimens was measured with a Cole-Palmer H–08406–46 infrared temperature measurement device. The woven 300 and 500 gm^{-2} glass fabrics and the aramid fibre-reinforced composite materials specimens were tested under different experimental conditions. Tests were conducted for speeds of 500 and 710 rpm and two different loads of 500 and 1000 g. Wear rate was determined by noting the weight loss (to 10^{-3} g) that was measured after the different sliding distances. One specimen was used for each experiment. The microstructures of the worn surfaces were examined by using a scanning electron microscope (SEM).

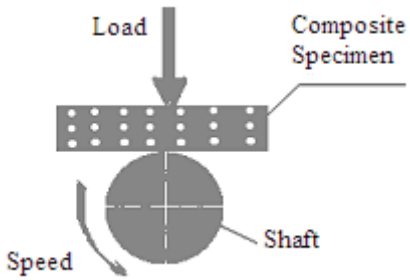

Fig. 1. Schematic showing a block-on-shaft wear test.

4. Experimental results and discussion

The effects of applied load and sliding speed on the weight loss of woven 300 and 500 glass fabrics and aramid fibre-reinforced composite specimens are shown in Figs. 2–3, respectively. The weight loss of the woven 300 glass fabric-reinforced composite specimens is lower than that exhibited by the woven 500 glass fabric-reinforced composite under the condition of 500 rpm speed and 500 g load (Fig. 2).

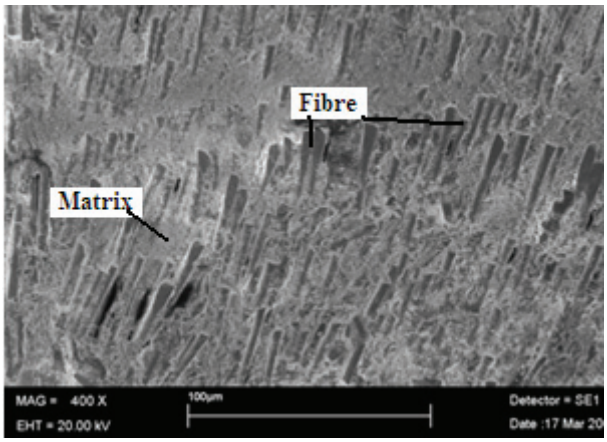

Fig. 2. SEM photograph showing the worn surface of the woven 500 glass fabric composite at 500 rpm speed and 500 g load.

The amount of matrix mass between fabrics in the woven 500 glass fabric-reinforced composite is more than that in woven 300 glass fabric-reinforced composite. For this reason, the reinforcement weight loss was very small, and weight loss was observed mainly as matrix loss. Epoxy-based composite exhibit lower wear loss than polyester-based composite [4,9]. The results also show that the wear did not occur in aramid fibre-reinforced composite specimens at 500 rpm speed and 500 g load, as shown in Fig. 2. Frequently, the wear and friction behaviour of polymeric composites have to be considered as a function of load, sliding speed and distance or temperature. The surface temperature plays an important role in the friction and wear of polymers. An increase in wear intensity can occur due to thermal softening. A low thickness of the softening layer normally results in low wear intensity [4]. From Figs. 2–3, it is seen that the wear increased with the increasing sliding distance. The weight loss of all the composite specimens generally increased depending on the sliding distance at the constant sliding speed 500 rpm when the applied load was increased from 500 to 1000 g (compare Fig. 3 with Fig. 2). The thickness of the softening polyester matrix layer on the specimen surface has increased proportionally with the temperature, so this softening layer has been detached from the surface of the specimens. The wear increased with an enhanced load, due to thermal softening [4]. As the earlier mentioned, epoxy-based composites exhibit lower wear loss than polyester-based composites.

In addition, aramid fibres usually exhibit much higher wear resistance than glass fibres [4,10] and aramid fibres exhibit lower friction than glass fibres. The low friction coefficient is prevented by the temperature increase. For this reason, the weight loss of the aramid fibre reinforced composite material is lower than that exhibited by the woven glass fabric-

reinforced composites. The weight loss of the woven glass fabrics and the aramid fibre reinforced composites increased by a small amount at the constant applied load (500 g) when the sliding speed was increased from 500 to 710 rpm (compare Fig. 4 with Fig. 2). The surface temperature is normally not independent of sliding speed [4]. The applied load on the specimens has more effect on the wear than the sliding speed according to the datas given in Figs. 2–4. The woven glass fabric-reinforced composites was subjected to a larger weight loss depending on sliding distance, when both the sliding speed and the applied load are increased together (Fig. 4). The surface temperature plays an important role in the friction and wear of polymers and increases at higher sliding speeds and loads [4]. The weight loss of the aramid fibre-reinforced composite had no change, as shown in Fig. 4.

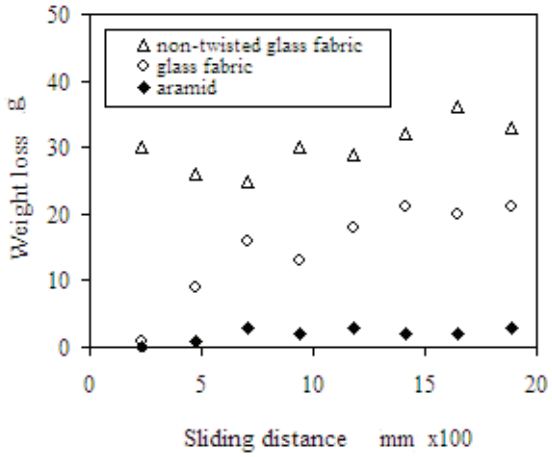

Fig. 3. Variation of weight lost with the sliding distances for 500 rpm speed and 1000 g load.

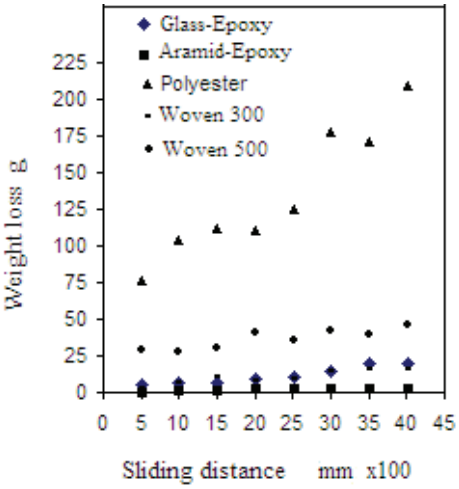

Fig. 4. Variation of weight lost with the sliding distances for 710 rpm speed and 1000 g load.

5. Drilling processes

In order to attain optimum results in drilling process, drilling length was chosed to be 15mm for the purpose of meeting the condition that drilling length should be three times or less than three times the hole diameter. Cooling liquid wasn't used in order to decrease possible heat shock in cutting tool during the experiment [11]. The experiments were done on the radial drill bench with a brand mane of Stanke Import with a progress interval of 0.056 mm/rev and 2, 5 mm/rev working between 20 and 2000 rpm. In drilling process, the effects of progress speed and number of rotations, drill type and drill peak angle, which are among the cutting parameters, on micro structure and surface roughness of work sample were investigated. In the experiments made, plastic matrixed composites manufactured in different ways were used. Some of the materials were supplied from TAI as semi-finished product. Various processes have been applied to these materials in order to use them in the experiments as products. Some other materials that were used in experiments by from (TEMSAN Turkish Elektromecanic Industry) as product. The composite materials used are shown in Table 1.

ISOVAL11- B	Epoxy / E-glass fiber	0.2 g/cm^3	3.5 mm
ISOVAL11- C	Epoxy / E-glass fiber	0.2 g/cm^3	5 mm
ISOVAL11- D	Epoxy / E-glass fiber	0.2 g/cm^3	7 mm
ISOVAL11- E	Epoxy / E-glass fiber	0.2 g/cm^3	10 mm
ISOVAL11- F	Epoxy / E-glass fiber	0.2 g/cm^3	14 mm

Table 1. The Composite Materials used in Experiments

5.1 ISOVAL11 composites

Final product with ISOVAL11 (Seen in Figure 5) series type and manufactured by TEMSAN has 0.2 g/cm^3 texture density. In Figure 6 the change in ISOVAL11 Epoxy/E-glass fiber composite and the average surface roughness is given for different drill materials. The biggest Ra value is found out for HSS drill material. In Figure 7 change in drill material

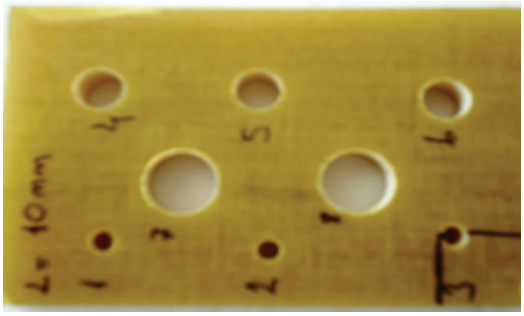

Fig. 5. ISOVAL 11 Composite materials used in experiments.

and the average surface roughness is given for ISOVAL11 Epoxy/E-glass fiber composite for different progress, rotation and drill diameters. In drills made at the same rotation and progress more sensitive surface is obtained in case Carbide drill is used and the same condition is applied for drills with 10 mm and 15 mm diameters. There is no heating on the

cutting tool where swarfs extracted occures as dust. It is seen that Ry value for the holes with 15 mm diameter is lower than the other. As material thickness increases, the linearity of the results are observed and the surface roughness is measured accurately.

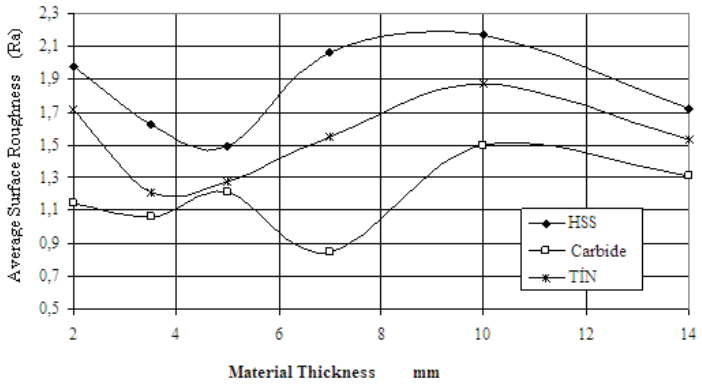

Fig. 6. The change in average surface roughness and ISOVAL11 Epoxy/E-glass fiber composite thickness. (s=0.112 mm/rot, n=250 d/min, d=10 mm).

In Figure 8 the SEM photos of middle point of hole section for ISOVAL11 Epoxy/E-glass composite drilled with HSS drill are shown. In these photos, the material texture denstity is 0.2 g/cm^3 and composite thickness is 5 mm, s=0.16 mm/rot, n=315 d/min, d=15 mm. In Kevlar materials, it is seen that the surface roughness is good in middle layers and roughness decreases in materials based on the texture condition. As material thickness increases extracting the swarf out during drilling become harder. As no cooling liquid is used during experimental studies, some heating occur on the cutting tool. Moreover as the material gets thicker it has difficulty in cutting the matrix material due to the fact that cutting tool is plastered over this region as matrix material per unit volıume increases and it is observed that heating occurs more in this region. The increased progress speeds and increased surface roughness values appear also as indicator of changes in texture condition of the material.

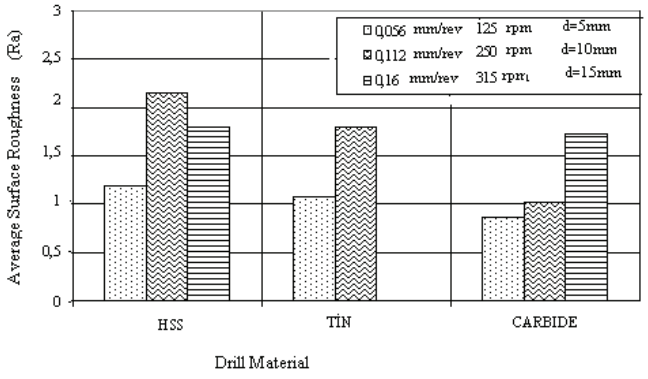

Fig. 7. The change in ISOVAL11 Epoxy/E-glass fiber composite and the average surface roughness (Texture density=0.2 g/cm^3, Composite material thickness=3.5 mm).

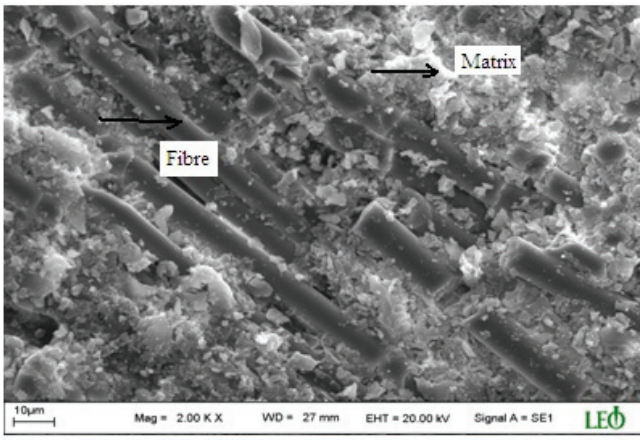

Fig. 8. 2000 times enlarged SEM photo of middlepoint of hole section for ISOVAL11 Epoxy/E-glass composite drilled with HSS drill (Texture density=0.2 g/cm^3, composite material thickness=5 mm, s=0.16 mm/rot, n=315 d/min, d=15 mm).

6. Conclusion

An experimental study of the wear behaviour of woven glass fabric and aramid fibre reinforced composites at various sliding speed, applied load and sliding distance reveals the following characteristics.

Wear of the composites depends on the experimental test parameters, such as applied load, sliding distance and speed. The applied load on the specimens has more effect on the wear than the sliding speed. The amount of matrix between fabrics in the woven 500 glass fabric-reinforced composite is more than in the woven 300 glass fabric. The wear occurs in the matrix rather than the reinforcement. Therefore, the wear in the woven 300 glass fabric-reinforced composite is lower than the woven 500 glass fabric-reinforced composite keeping all test parameters constant. Due to the aramid fibres having a low friction coefficient and high wear strength, and epoxy-based composite exhibit lower wear loss than polyester-based composite, the wear of the aramid fibre-reinforced composite is lower than the woven glass fabric-reinforced composites.

The surface roughness of the composite material is investigated experimentally depending on the effect of drill type, drill diameter, number of rotation and progress speed on machinability of different composite materials in drilling.

Since no cooling liquid is used, as a result of the heating occured around the hole matrix material gets softer. Due to this, in drilling processes with all drills there is matrix concentration on the edges of hole surfaces. Sudden ruptures occur between the textures on composite materials as progress speed increases and the value of surface roughness is seen to increase in all study in general.

Considering the value of surfaceroughness depending on the number of rotation, in all drilling processes made with drills it is observed that the value of surface roughness increases as the number of rotation increases. As material thickness increases in general, the surface roughness increases; naturally drilling becomes difficult and tool heat increases as well. It was previously stated that when an investigation is made among the materials, the

rupture endurance of material with Kevlar support is higher than that of fiber glass material. Due to this it is seen that drilling Kevlar supported material is more difficult. Considering all results obtained as a result of the drilling processes; it is found out that using Carbide drills as the most suitable drill type in drilling operations would create better results. Besides this, considering the cost, as the price of Carbide drills is twice as expensive as TIN covered drills which have a similar performance as Carbide drills, it can be reccommendable that TIN covered drills to be used.

7. References

[1] Pihtili,H.,Canpolat,N., Investigating of Surface Roughness and Capability of Being Drilled of Different Reinforced Composite Materials, Journal of Composite Materials,Volume 43 Issue 19, 2070-2080, 2009.

[2] Pihtili, H.,N.Tosun, Investigation of the wear behaviour of a glass fibre-reinforced composite and plain polyester resin, Composite Sci. Technol. 62 (3) 367–370, 2002.

[3] N.S. El-Tayep, R.M. Gadelrap, Friction and wear properties of E-glass fiber reinforced epoksi composites under different sliding contact conditions, Wear 192 112–117, 1996.

[4] K.H. Zum Gahr, Microstructure and wear of materials, Tribology Series, Vol. 10, Elsevier, Amsterdam, 1987.

[5] B. Vishwanath, A.P. Verma, C.V.S. Kameswara Rao, Composite Sci. Technol. 44 (1) 77–86, 1992.

[6] Schaefer W.H., Christion J.L., "Evaluation of the structural behaviour of filament reinforced metal matrix composites", Technical report No. AFML-TR-69-36, vol. 3, air Force Materials Laboratory, 1969

[7] M.R. Piggot, Load-Bearing Fibre Composite, Pergamon Press, Oxford, 1980.

[8] P.K. Mallick, Fiber-Reinforced Composites: Materials, Manufacturing, and Design, Marcel Dekker, New York, 1988.

[9] N. Chand, M. Fahim, S.G. Hussain, Effect of 60Co gamma-irradiation on interface and abrasive wear of glass-reinforced polyester composite, J. Mater. Sci. Lett. 12 (1993) 1603- 1605.

[10] S.N. Kukureka, C.J. Hooke, M. Rao, P. Liao, Y.K. Chen, The effect of fibre-reinforcement on the friction and wear af polyamide 66 under dry rolling–sliding contact, Tribol. Int. 32, 107–116, 1999.

[11]Durante, S., Rutefli, G., Rabezzana, F., Aluminum-based MMC machining with diamond-coated cutting tools, Surface & Coatings Technology, 94-95 (1-3), 632-640, 1997.